HHS Public Access

Author manuscript

Nat Immunol. Author manuscript; available in PMC 2024 September 01.

Published in final edited form as:

Nat Immunol. 2023 September ; 24(9): 1511–1526. doi:10.1038/s41590-023-01590-2.

Baseline innate and T cell populations are correlates of protection against symptomatic influenza virus infection independent of serology

Robert C. Mettelman[1,#], **Aisha Souquette**[1,#], **Lee-Ann Van de Velde**[1], **Kasi Vegesana**[1], **E. Kaitlynn Allen**[1], **Christina M. Kackos**[2], **Sanja Trifkovic**[2], **Jennifer DeBeauchamp**[2], **Taylor L. Wilson**[1,3], **Deryn G. St. James**[1,3], **Smrithi S. Menon**[1], **Timothy Wood**[4], **Lauren Jelley**[4], **Richard J. Webby**[2,*], **Q. Sue Huang**[4,*], **Paul G. Thomas**[1,*],

SHIVERS-II Investigation Team

[1]Department of Immunology, St. Jude Children's Research Hospital, Memphis, TN, United States

[2]Department of Host-Microbe Interactions, St. Jude Children's Research Hospital, Memphis, TN, United States

[3]Department of Microbiology, Immunology, and Biochemistry, College of Graduate Health Sciences, University of Tennessee Health Science Center, Memphis, TN, United States

[4]Institute of Environmental Science and Research Limited (ESR), Wallaceville Science Centre, Upper Hutt, NZ

Abstract

Corresponding Authors: Please direct correspondence to Richard J. Webby, Q. Sue Huang, or Paul G. Thomas.

[#]These authors contributed equally

Robert C. Mettelman and Aisha Souquette (co-first)

Lee-Ann Van de Velde and Kasi Vegesana (co-second)

[*]These authors jointly supervised this work

Richard J. Webby, Q. Sue Huang, and Paul G. Thomas

Consortia: The SHIVERS-II Investigation Team

Judy Bocacao[1], Jacqui Ralston[1], Jessica Danielewicz[1], Wendy Gunn[1], Nayyereh Aminisani[1], Ben Waite[1], R. Pamela Kawakami[1], Annette Nesdale[2], Michelle Balm[2], Nikki Turner[3,4], and Tony Dowell[5]

[1] Institute of Environmental Science and Research Limited (ESR), Wallaceville Science Centre, Upper Hutt, NZ

[2] Te Whatu Ora Health New Zealand (Capital, Coast and Hutt Valley), Wellington, NZ

[3] Department of General Practice and Primary Health Care, School of Population Health, University of Auckland, NZ

[4] Immunisation Advisory Centre, University of Auckland, NZ

[5] Department of Primary Health Care and General Practice - University of Otago, Wellington, NZ

Contributions

Conceptualization: R.C.M., A.S., R.J.W, Q.S.H., and P.G.T. Formal analysis: R.C.M., A.S., L.A.V., and K.V. Investigation: R.C.M., A.S., L.A.V., K.V., E.K.A., T.L.W., D.G.S, S.M.M., C.M.K., J.D., and S.J. Methods development: R.C.M., A.S., L.A.V., K.V., E.K.A., T.L.W., C.M.K., J.D., and S.J. Resources: T.W., L.J., and Q.S.H. Data and sample curation: T.W., L.J., Q.S.H, and the SHIVERS-II Investigation Team. Writing, original draft: R.C.M. and A.S. Writing, review, and editing: R.C.M., A.S., L.A.V., K.V., E.K.A., R.J.W., Q.S.H., and P.G.T. Visualization: R.C.M., and K.V. Supervision: R.J.W., Q.S.H., and P.G.T. Funding Acquisition: R.C.M., R.J.W., Q.S.H., and P.G.T.

CODE AVAILABILITY

A minimum dataset containing de-identified study participant information and biological assay results along with custom study-generated R code for analysis was uploaded to GitHub (https://github.com/kvegesan-stjude/SHIVERS2) per the data sharing agreement stipulated under the NRSA-NIAID Individual Postdoctoral Fellowship award number F32AI157296 (R.C.M). Additional basic R code can be made available upon reasonable request.

Study Ethics Statement. This study received ethics approval from the New Zealand Health & Disability Ethics Committee (NTX11.11.102.AM36 & AM36 & AM49 & AM51). All participants provided written consent to participate in the study. De-identified participant samples (PBMC, serum) and associated demographic information were provided under the St. Jude Children's Research Hospital Center of Excellence for Influenza Research and Surveillance NIAID contract #HHSN272201400006C.

Evidence suggests innate and adaptive cellular responses mediate resistance to influenza virus and confer protection after vaccination. However, few studies have resolved the contribution of cellular responses within the context of pre-existing antibody titers. Here, we measured peripheral immune profiles for 206 vaccinated or unvaccinated adults to determine how baseline variations in cellular and humoral compartments contribute independently or synergistically to the risk of developing symptomatic influenza. Protection correlated with diverse and polyfunctional CD4 and CD8 T cells, cTfh, mDCs, Th17 cells, and $CD16^{+}$ NK cell subsets. Conversely, increased susceptibility was predominantly attributed to nonspecific inflammatory populations, including γδ T and activated $CD16^{neg}$ NKs, as well as $TNF\alpha^{+}$ single-producing CD8 T cells. Multivariate and predictive modeling indicate cellular subsets i) work synergistically with humoral immunity to confer protection, ii) improve model performance over demographic and serologic factors alone, and iii) comprise the most important predictive covariates. Together, these results demonstrate that pre-infection peripheral cell composition improves prediction of symptomatic influenza susceptibility over vaccination, demographics, or serology alone.

INTRODUCTION

Influenza viruses are among the leading etiologic agents responsible for human respiratory illness with annual infection estimates between 10–49 million and upwards of 650,000 deaths globally[1,2]. Although seasonal influenza vaccinations are an important preventative measure limiting severe disease, year-to-year effectiveness is inconsistent ranging between 10–60%[3–7]. Some of this variability is attributable to incomplete matching between circulating and vaccine strains, but another possible factor is the reliance on these vaccines to generate protective humoral immunity alone. While current seasonal influenza vaccine platforms can promote robust antibody titers and the helper T cell responses necessary to promote them, none are specifically designed to stimulate durable, virus-specific cellular immunity, thereby neglecting a potential ally in preventing and controlling influenza virus infection. In recent years, there have been several large-scale initiatives to improve influenza vaccine design by increasing surveillance and strain prediction, identifying universal humoral or T cell antigens, evaluating new delivery platforms, and considering demographic-specific formulations[8–11]. Driving this push is the need to understand the complete range of protective immune responses limiting symptomatic influenza illness – termed correlates of protection (CoP) – which to date have been largely defined by serologic measurements alone. Few studies have examined how efficacious serological data are as predictors of influenza protection within the context of additional immune measures, such as cellular and innate immunity, how individual cell populations contribute to protection in the presence of existing antibody responses, or if/how these compartments coordinate.

Further complicating the study of CoP against influenza viruses is the substantial degree of baseline immune variation that exists across humans, now recognized as a key determinant in predicting efficacy of some vaccines and therapeutics, and modeling disease outcomes[12–17]. Differences in host genetics, environmental and demographic factors, and antigen exposure histories impact the composition of baseline innate, cell-mediated immune (CMI; adaptive T cells), and humoral compartments, and may augment varied responses to influenza virus infection or vaccination[15,18–31]. Therefore, identifying baseline CoP

necessitates the use of large, well-curated, influenza virus-seropositive human cohorts where immune and demographic data are considered together. To address these challenges, the second iteration of the Southern Hemisphere Influenza Vaccine Effectiveness and Response Study (SHIVERS-II) was established to track unvaccinated and vaccinated adults within a natural community setting in New Zealand. Using baseline serum and peripheral blood samples from 206 SHIVERS-II adult participants, we aimed to define baseline immune cell subsets correlated with protection against symptomatic influenza independently from or synergistically with humoral responses. Further, we investigated the quantitative and relative contributions of baseline cellular and humoral compartments in mediating protective anti-influenza virus immunity. Our analytic approach incorporates high-dimension flow cytometry, serology measures, vaccination status, and demographic data into statistical models allowing identification of individual baseline cell populations associated with increased risk or protection against symptomatic influenza across vaccinated and unvaccinated adults, while accounting for baseline immune and demographic variation. Using univariate analyses and multivariate partition and regression models, we demonstrate that baseline composition of peripheral cell profiles improves influenza susceptibility risk prediction over serology, vaccination, or demographics alone. Our results underscore the complexity and variability of baseline cellular responses, support influenza vaccine design strategies targeting optimized cell subsets to induce long-lasting heterosubtypic immunity, and provide improved methods to compare vaccine effectiveness.

RESULTS

Study Population

A total of 206 adult subjects (Table 1) were selected from the 2018 SHIVERS-II cohort for inclusion in this study (Fig. 1a) and were analyzed according to pre-defined analysis pipeline (Extended data figure 1). Participant selections were divided into four roughly age- and sex-matched comparator groups based on influenza virus vaccine and infection status: vaccinated-uninfected (n=75), vaccinated-infected (n=33), unvaccinated-uninfected (n=76), unvaccinated-infected (n=22; Fig. 1b). Participant age was comparable across sex and vaccine status reducing the potential for confounding effects due to sample selection bias (Fig. 1c). Baseline serum and peripheral blood mononuclear cells (PBMCs) were collected pre-season (March-May) for unvaccinated participants or 14 days-post vaccination for vaccinees. Post-season serum samples were collected September through January with a majority sampled in November. All participants exhibiting respiratory symptoms meeting World Health Organization (WHO)-defined criteria for influenza-like illness (ILI) were further tested by PCR. Participants presenting with ILI and an associated influenza-positive PCR result were defined as ‘symptomatic’ influenza cases. For the 2018 influenza season (May-September), 41 of 55 (74.5%) influenza virus infections were symptomatic with a majority attributed to A(H1N1) (n=29, 70.7%), though infections with A(H3N2) (n=5, 12.2%), B/Yamagata lineage (n=1, 2.4%), B/Victoria lineage (n=1, 2.4%), and influenza A without subtype (n=5, 12.2%) viruses were also recorded (Supplementary Table 1). Cryptic influenza cases, identified by seroconversion (≥4-fold rise in anti-HA inhibiting antibody titer ≥1:40) in the absence of an influenza PCR-confirmed symptomatic episode, comprised the other 14 of 55 (25.5%) infections. Influenza virus strains associated with infection were

proportional across male and female participants (Fig. 1d). Supplementary Tables 1–2 detail participant vaccination status and demographics by influenza virus strain.

Baseline serology measures associate with protection

Anti-influenza virus antibodies targeting hemagglutinin (HA) and neuraminidase (NA) are known CoP[32–37]. To determine the degree of pre-existing humoral immunity to dominant influenza viruses circulating in the region as well as those present in the 2018 quadrivalent influenza vaccine[38–40], we measured inhibiting antibody titers by inhibition assays (HAI; NAI) and total binding antibody by ELISA. Overall correlation between inhibiting and total anti-HA (Fig. 2a) or anti-NA (Fig. 2b) serology measures against homosubtypic influenza virus targets were positive reflecting a large degree of concordance between the assays. Three correlation clusters were also identified across all serology measures (Extended data figure 2a) suggesting association between existing anti-influenza antibody responses to homo- and heterosubtypic targets. In 2018, the quadrivalent influenza vaccine was 38% effective at preventing influenza-associated hospitalizations[40]. In our study, this vaccine elicited HAI titers ≥1:40, a purported cutoff for protection, in roughly half of study participants sampled 14 days-post immunization (Extended data figure 2b). Vaccinated participants exhibited significantly increased HAI and NAI titers compared to the unvaccinated against all targets (Fig. 2c–d). ELISA results depicting total binding antibody were also significantly increased in vaccinees, apart from B/Victoria (lineage) HA and A(N2), which were lower than in unvaccinated (Fig. 2e–f). Further, we compared antibody levels in uninfected and cryptic influenza to symptomatic influenza cases. For these and other downstream analyses, uninfected and cryptic infection cases were grouped together as these participants did not meet study criteria for symptomatic influenza and represent a more protected group. Nearly all NAI titers were significantly increased in the uninfected/cryptic group (Fig. 2h), while only total anti-A(H1) and anti-B/Yamagata (lineage) NA binding antibody levels were increased in uninfected/cryptic (Fig. 2 i–j).

Previous studies suggest demographic factors can influence humoral responses, illness susceptibility, and influenza vaccine effectiveness[19,41–43]. Therefore, we looked for correlations between age, sex, or BMI across serology measures using locally estimated scatterplot smoothing (LOESS) to inform downstream statistical modeling. Although age and BMI were not correlated with participant sex (Extended data figure 2c), we did observe significant relationships between age and BMI with several serology measures (Extended data figure 2d–k). While these results indicate the effect of demographics on antibody levels is limited to specific targets, this variability may influence serology measures in downstream modeling and was therefore accounted for.

As higher antibody titers were observed in the uninfected/cryptic group, we used generalized logistic regression modeling (GLM) to establish risk of symptomatic influenza virus infection given individual serology measures while adjusting for demographics and influenza vaccine status. Elevated NAI titers against A(N1), A(N2), B/Victoria (lineage) NA and B/Yamagata (lineage) NA, and total binding antibodies targeting A(H1) and B/Yamagata (lineage) HA were significantly associated with protection (OR<1; Fig. 2k–l). In line with the elevated HAI titer observed in symptomatic influenza cases (Fig. 2g),

increased risk (OR>1) was associated with elevated A(H3) HAI titer (Fig. 2k). This likely reflects the dominance of regional A(H3N2) virus infections the year prior (2017)[44] skewing pre-existing antibody levels away from an effective titer needed to neutralize the A(H1N1) viruses circulating during 2018[40]. Together, the serology results from SHIVERS-II are consistent with numerous studies demonstrating protection mediated by anti-influenza antibodies. Further, these results suggest that baseline levels of anti-NA inhibiting antibodies are particularly important in determining risk of symptomatic influenza infection in this cohort.

Immune measures vary across vaccine and infection status

As our subjects are relatively evenly divided by vaccination status, this allowed us to observe the statistical behavior of all variables separately across vaccination and infection groups. Statistical differences in individual baseline demographic, serologic, and cellular covariates were evaluated between participants with and without symptomatic infection and presented in Supplementary Table 3. Regardless of vaccination and infection status, no significant differences in demographic parameters (age, sex, BMI, ethnicity) were observed (Supplementary Table 3). For serology measures, unvaccinated participants in the uninfected/cryptic infection group had higher median values of total A(H1) and B/Yamagata (lineage) NA binding antibodies and NAI titers against B/Yamagata (lineage), while median A(H3) HAI titer was elevated in symptomatic influenza cases (Supplementary Table 3). Regardless of vaccine status, higher median NAI titers of A(N1), A(N2), and B/Victoria (lineage) were observed in the uninfected/cryptic group (Supplementary Table 3).

To evaluate variations in baseline cell profile across participants, PBMCs were stained with fluorescent antibody panels distinguishing a wide array of phenotypic and functional myeloid (Extended data figure 3) or lymphoid cell subsets (Extended data figure 4). To promote influenza virus-specific cytokine production for functional intracellular cytokine staining (ICS) in the lymphoid panel, a portion of participant PBMCs were stimulated with conserved influenza virus peptide pools or live A(H1N1) or A(H3N2) viruses. Across vaccinated and unvaccinated participants, 11 cell populations were significantly increased in uninfected/cryptic cases (Supplementary Table 3). Conversely, 20 cell populations were significantly increased in symptomatic infection cases. While some of these cell populations were elevated regardless of vaccine status, the overall cell profiles were distinct suggesting an effect of immunization on protective or susceptible cellular profiles.

Predictive baseline cell profiles differ by vaccine status

To define cellular CoP against symptomatic influenza, cell populations were then evaluated by univariate GLM, with respect to vaccination status, to determine whether baseline cell population frequencies were associated with a change in the relative risk of acquiring symptomatic influenza during the 2018 season (Fig. 3a; Supplementary Table 4). We identified 14 cell populations with significant protective associations (OR<1) within vaccinated (myeloid dendritic cells [mDC]; naïve CD4 T cells; effector CD4 and CD8 T cells; dual cytokine-producing [IL2/TNFα/IFNγ] CD8 and CD4 T cells; CD4 $PD1^+$; total circulating T follicular helper [cTfh]; cTfh $ICOS^+$; cTfh $CXCR3^+$; total CD8 T cells) and unvaccinated (myeloid DC [mDC]; cytotoxic natural killer [NK]; cytokine-producing NK;

naïve CD4 T cells; CD4 Th17; total CD8 T cells) subjects (Fig. 3a). We also resolved 7 populations that increased risk of symptomatic influenza (OR>1) among vaccinated (plasmacytoid dendritic cells [pDC]; NK GzmB^{+}IFNγ^{neg}; activated NK; γδ T cells; CD8 memory CCR5^{+}) or unvaccinated (activated NK; γδ T cells; CD8 memory CCR5^{+}; total CD4 T cells; CD8 TNFα^{+}) participants (Fig. 3a). The overall cellular correlate of protection profile defined by the univariate analyses indicates a diversity of polyfunctional responses to influenza viruses, engaging both the adaptive and innate compartments (Fig. 3b; **left**). In contrast, the susceptible-associated profile skewed toward non-specific inflammatory and single cytokine-producers (Fig. 3b; **right**). Comparison of cell profiles from unvaccinated participants across protective and non-protective status also indicates that baseline composition of innate populations is an important determinant of protection from symptomatic influenza in the absence of recent vaccine-induced immunity.

ROC thresholds define protection and susceptibility cutoffs

From the univariate analyses, we identified individual immune measures associated with protection from or increased risk of developing symptomatic influenza. To provide a quantitative value denoting protection or susceptibility we derived ‘threshold’ values for each cell population (Supplementary Table 5) or serology measure (Supplementary Table 6) using receiver-operating characteristic (ROC) analysis. Thresholds define the value at which an individual parameter accurately identifies ~50% of true positive cases (sensitivity), while minimizing false positives (specificity). Therefore, a threshold is a quantifiable measure at and above which a factor accurately associates with protection or susceptibility. The area under the ROC curve (AUC) defines the quality of the immune measure as a classifier. For example, a baseline frequency of CD4^{+} dual cytokine-producers above a threshold of 0.022% identifies at least 50% of vaccinated individuals protected from symptomatic influenza (Fig. 3c). Conversely, a threshold frequency ≥12.7% Activated NKs correctly identifies at least 50% of individuals susceptible to symptomatic influenza (Fig. 3c). Comparing the protection-associated factors with the highest AUC values (Supplementary Table 5–6) we observed that serology measures were more accurate in classifying cases in unvaccinated participants (e.g. NAI B/Yamagata (lineage) AUC = 0.9; NAI B/Victoria (lineage) AUC = 0.86; NAI A(N1) AUC = 0.85), while cellular measures were more accurate in vaccinated participants (e.g. CD4 (Dual CK) AUC = 0.78; CD4 (IL2^{+}) AUC = 0.77; cTfh (ICOS^{+}) AUC = 0.77). This is likely because overall antibody levels are elevated in vaccinated individuals so differences in cell populations provide improved resolution; in unvaccinated individuals increased baseline antibodies are more variable and therefore more accurate classifiers likely reflecting a more recent exposure to influenza antigen. However, as these are single parameter measures, we cannot determine from the AUC values alone if other confounding factors impact these classifications.

Cryptic influenza cases associated with unique cell profiles

Susceptibility to symptomatic influenza comprises risks associated with i) virus exposure and ii) symptom development following exposure. Outside of regional prevalence estimates, it was difficult to determine if uninfected study participants were indeed exposed to influenza viruses during the 2018 season. Therefore, we analyzed a subset of participants with confirmed exposures: symptomatic influenza (confirmed by PCR; n=41) and cryptic

infection (confirmed by seroconversion; n=14) cases. Univariate regression analyses demonstrated that elevated baseline levels of several anti-HA or anti-NA inhibitory or total binding antibody measures were significantly associated with reduced risk of symptomatic influenza, while demographic factors and recent influenza vaccine history were not (Fig. 4a). We then compared cell frequencies between symptomatic and cryptic cases. In concordance with our univariate results, both activated and GzmB^{neg}IFNγ^+ NKs were increased at baseline in symptomatic cases further suggesting a role in susceptibility (Fig. 4b). Conversely, we identified 15 cell populations with increased baseline frequencies in cryptic infection cases comprising a unique set of protective responses, including several (conventional DC type 2 [cDC2] and cTfh IL21$^+$) not identified in the prior univariate analysis (Fig. 4c). Like the univariate protective profile, baseline cell populations increased in cryptic cases were diverse and polyfunctional, reflecting adaptive T cell activation and cytokine production (CD4 effector; CD4 IL17$^+$; CD4 IL2$^+$; CD8 IL2$^+$; CD8 IFNγ^+; CD8 dual-cytokine), engagement with humoral immunity (cTfh subsets), and innate immune activities (cytotoxic and cytokine-producing NK, mDCs).

Immune cell populations cluster into co-regulated modules

The above univariate analyses consider cell populations independently and do not account for coordinated responses often observed across adaptive and innate immune compartments. We sought to understand the cell-cell relationships within our dataset and determine which populations represented co-regulated immune cell modules, defined here as cell populations with strong positive correlation in cell frequencies suggestive of parallel responses. Using Pearson's bivariate correlation, we identified 9 myeloid (Fig. 5a) and 13 lymphoid/functional (Fig. 5b) cell modules across all study participants. We also evaluated immune cell correlations in vaccinated and unvaccinated participants separately (Extended data figure 5) and found them to largely reflect the same correlation groups identified from the complete set of subjects. Correlation results from the complete set of participants were used for downstream analyses. The cell frequencies from individual populations within a given module were averaged to give final "Cluster" frequency values, which were compared by influenza virus infection status. Clusters with increased average cell frequencies in both influenza negative or cryptic infection cases included myeloid Clusters 1 (mDC; CD14$^+$CD16$^+$ intermediate monocytes), 3 (cytotoxic and cytokine-producing NK; neutrophils), and 8 (cDC2; Fig. 5c), and lymphoid/functional Clusters 4 (TNFα^+, IFNγ^+, IL17$^+$, and dual cytokine-producing [IL2/TNFα/IFNγ] CD4 T cells; IFNγ^+ and dual cytokine-producing [IL2/TNFα/IFNγ] CD8 T cells), 8 (CD4 and CD8 effector T cells), 9 (PD1$^+$ CD4, CD8, and cTfh; CXCR3$^+$ cTfh cells), and 13 (total CD8, GzmB$^+$ CD4 and CD8, $\gamma\delta$ T cells; Fig. 5d). Conversely, myeloid Cluster 7 (activated NKs) was found to be increased in symptomatic cases (Fig. 5c), supporting the previous observations made in the univariate GLM analysis. Together, these results reflect the involvement of coordinated cellular responses in determining influenza virus susceptibility in cases of confirmed exposure.

Immune cells most accurately categorize influenza cases

By defining the univariate cellular CoP and susceptibility through regression modeling, we have shown the individual contributions of baseline innate and adaptive T cell populations

in mitigating or enhancing symptomatic influenza. We next sought to provide additional context to these cellular responses by determining which covariates, spanning demographic, vaccine, serology, and immune cell categories, would best predict future infections during the 2018 influenza season. To do this, we built, trained, and compared random forest models from an 80:20 (train:test) split of 200 participants, ensuring equivalent proportions of cases (symptomatic influenza) and controls (uninfected and cryptic influenza). Four random forest models were built including: (i) Base Model predicting symptomatic infection from demographic, 2018 influenza vaccine status, and serology covariates; (ii) Lymphoid Model comprising lymphoid/functional panel cell frequencies and all Base variables; (iii) Myeloid Model comprising myeloid panel cell frequencies and all Base variables; (iv) Combined Model comprising all available variables. Model performance was measured by sensitivity and specificity metrics and by scoring data from the testing set in ROC curves (Fig. 6a). While we observed that both the Base and Myeloid Models categorized participants with 79% accuracy (Fig. 6a; **bottom right**), the Lymphoid Model increased sensitivity and specificity and substantially improved categorization accuracy to 86% demonstrating the influence of lymphoid populations in categorizing influenza cases. As the Combined Model (84% accuracy) did not improve accuracy over the Lymphoid Model, we probed the relative contributions of lymphoid and myeloid populations in model performance. Three additional random forest models, including Myeloid Only, Lymphoid Only, and combined Lymphoid+Myeloid, were also built, trained, and compared (Extended data figure 6). The Lymphoid Only model (79%) performed better than the Myeloid Only (72%) and was as accurate as the Base Model (79%) in classifying symptomatic influenza cases. The combination Lymphoid+Myeloid model also exhibited higher accuracy (81%) than the Base model. These data indicate that lymphoid populations improve overall accuracy in classifying symptomatic influenza cases compared to myeloid populations, serology, vaccine status, and demographics alone. Using Variable Importance (VIP) analysis of the Combined Model, we then derived ‘importance’ values representing the individual effect strength on the dependent variable. Strikingly, the top 4 (and 25 of the top 30) most important covariates used in categorizing symptomatic and uninfected/cryptic influenza cases were of cellular origin with cTfh ICOS$^+$ cells being of the highest importance (Fig. 6b). Indeed, cTfh ICOS$^+$ frequency was significantly higher in uninfected/cryptic influenza cases across both unvaccinated and vaccinated participants (Fig. 6c) and had a predictive accuracy of 81.6% following cross-validation and adjustment for age, sex, and vaccine status (Fig. 6d). Together, the results from the partition analyses emphasize the strong contributions of both baseline innate and adaptive cellular immunity in regulating responses to influenza virus and mitigating symptomatic disease.

Baseline immune measures predict influenza susceptibility

While partition analysis helps determine which combined or individual baseline variables best categorize symptomatic and uninfected/cryptic participants, these models are limited in risk assessment. Indeed, the random forest and VIP analyses here do not ascribe effect directionality nor associate any factor with increased or decreased risk of symptomatic influenza. Therefore, we turned to GLM regression modeling to assess influenza risk given all measures of immune and demographic variation present at baseline. A multivariate GLM was constructed to identify the differential effects of cell populations, anti-influenza virus

antibodies, vaccine status, and demographics on determining overall risk of symptomatic influenza (Fig. 7). GLMs with highly correlated factors (collinearity) often produce unreliable coefficients with high standard errors[45]. Due to the high dimensionality and observed correlation between the cellular and serology immune measures in our data, we took several steps to reduce variable collinearity (Pearson's correlation and variance inflation factor) and optimized selected covariates by comparing stepwise models using Akaike information criterion (AIC) and Bayesian model averaging (BMA) (Extended data figure 1). The final multivariate GLM was constructed using the set of selected covariates against a response variable denoting symptomatic infections (Fig. 7a). The model comprises 19 covariates, 4 (CD4 CD107a$^+$; intermediate monocytes; NAI A(N1) and B/Victoria (lineage)) with significant association with protection and 2 (CD8 TNFα$^+$; γδ T cells) that significantly predict increased risk of symptomatic influenza. Using CD4 CD107a$^+$ as an example, the GLM readout shows that for each 4.2% increase in CD4 CD107a$^+$ frequency, the odds associated with developing symptomatic infection decrease by 11.1-fold (1/0.09). Although neither age (p=0.051) or 2018 vaccine status (p=0.859) had significant effects on risk, these variables were included in the GLM to account for variability across participants. Due to strong correlations observed among cell populations, we can further infer protection or susceptibility associations by identifying the myeloid or lymphoid modules these populations reside within (Fig. 7b) and referencing the univariate associations for a given cell population (Fig. 3b). Together, the final GLM results indicate that baseline serologic and cellular factors, when considered together, synergistically predict influenza virus infection outcomes and contribute to the relative risk of developing influenza disease. Results from this study support recent calls to target adaptive T cell populations in next-generation vaccine designs[11] and strongly suggest that both cellular and serology measures are necessary to fully assess efficacy of influenza vaccines.

DISCUSSION

Immune responses to influenza viruses are complex and include coordinated innate, CMI, and serologic responses to clear active infections, build durable immune memory, and rapidly neutralize subsequent challenges. Equally nuanced are the determinants of risk and susceptibility to symptomatic influenza, which comprise individual comorbidities and demographic risk factors, vaccination and infection histories, and variations in baseline immune profiles. In our study, we asked which baseline immune cell populations affected risk of developing symptomatic influenza, and probed how differences in pre-existing anti-influenza virus antibody titers, influenza vaccination status, and participant-level demographics impacted these associations.

Our univariate analyses demonstrate that protection from symptomatic influenza correlates with increased frequencies of diverse and polyfunctional influenza virus-specific CD4 and CD8 T cells, cells associated with engagement of humoral responses including cTfh, mDCs, and Th17 cells, and innate immune effector CD16$^+$ cytotoxic and cytokine-producing NKs, many of which have been observed in other studies. As expected, protection profiles were distinct between vaccinated and unvaccinated adults. The vaccine-associated protective profile favored effector and polyfunctional adaptive populations pointing toward influenza virus-specific T cell activation. Elevated antigen-presenting mDCs

and cTfh populations in vaccinees were also suggestive of humoral crosstalk, discussed in detail below. In unvaccinated subjects, protection was associated with increased baseline populations exhibiting analogous, albeit antigen-agnostic, functions to those observed following vaccination. For example elevated Th17 cells, which were protective in our study, have been shown to be involved in anti-influenza virus responses either directly[46], through B cell engagement promoting IgG, IgA, and IgM[47,48], or by recruiting pre-existing B cells into the lung without vaccine priming[48–50]. Therefore, Th17 cells may compensate for the absence of other vaccine-induced CD8 or CD4 T helper subsets. Cytokine-producing and cytotoxic NKs exhibiting virus-limiting potential similar to CD8 T cells, were also strongly protective in unvaccinated subjects supporting studies demonstrating active roles for NKs in anti-influenza virus responses and limiting disease severity[51–58]. NKs, however, may also be a double-edged sword. One group reported a link between IFNγ-producing NKs and extrapulmonary inflammation leading to poor outcomes in influenza virus-infected pregnant women[59]. Coinciding with these findings, we also observed increased risk of symptomatic influenza in participants with elevated baseline frequencies of activated NKs ($CD56^{dim}HLA\text{-}DR^{hi}CD16^{neg}$), suggesting pleiotropic roles for NKs during influenza virus infection.

A main takeaway from this study is the importance of cell-humoral crosstalk promoting increased baseline levels of anti-influenza virus antibodies. We report that elevated baseline NAI titers were the best serology predictors of symptomatic influenza and associate with protection, supporting other recent findings[34–36,60–62]. However, we also found that addition of lymphoid cell populations improved prediction of symptomatic influenza cases arguing that baseline antibody levels cannot be considered alone. Indeed, sustained B-T cell crosstalk within germinal centers as well as cTfh cells in peripheral blood are associated with productive anti-influenza virus humoral response[63–67]. In our study, evidence of this communication is supported by the association of CD4 populations, including cTfh subsets, with protection. In fact, cTfh $ICOS^+$ cells represent the most important variable in determining Combined Model accuracy. From our analysis of co-regulated cell modules, we found cTfh $ICOS^+$ cells correlated with CD4 and CD8 memory T cell populations (Lymphoid Cluster 11) linking increased cTfh $ICOS^+$ frequency to long-term memory. We also identified correlations across Th17, IFNγ^+, and polyfunctional CD4 and CD8 T cells (Lymphoid Cluster 4), which are known to improve outcomes during influenza virus infection[68]. Further, our multivariate regression modeling identified reduced risk of symptomatic influenza is independently associated with $CD107a^+$ CD4 T cells, $CD14^+CD16^+$ intermediate monocytes, and anti-influenza virus NAI titers targeting A(H1N1) and B/Victoria (lineage) viruses. CD107a is a marker of degranulation[69] and implies that these CD4 T cells were specifically activated by influenza virus antigens during ICS and flow cytometry. That these populations are observed at baseline indicates that cTfh and other influenza-responsive T cells persist following influenza antigen exposure in prior seasons and may confer ‘carryover’ protection in a subset of participants[70]. However, as our study was limited to immune measures present in circulation, we did not evaluate contributions from mucosa-associated cells, secretory IgA, or IgG produced by respiratory-resident memory B cells, likely CoP (reviewed in[24,71]). As cTfh $ICOS^+$ and other functional lymphoid cells rank highly in our study, we hypothesize that cellular correlates might

provide better insights towards mucosal immune responses (including antibody) compared to serum antibody measures.

A strength of our statistical modeling approach is the ability to define not only CoP, but also baseline factors that increase risk of symptomatic influenza. Among the strongest risk-associated cell populations identified across univariate and multivariate models were γδ T cells. A prior study from our group demonstrated that γδ T cells are integral for lung repair in neonatal mice[72]; however, in this adult SHIVERS-II cohort, the opposite effect was observed. This incongruence could be attributed to differences in γδ TCR repertoires, which change significantly with age, tissue-localization, and infection history[73,74]. While pediatric γδ T cells exhibit non-overlapping TCR repertoires, adult γδ T cells heavily favor Vγ9 and Vδ2 chain usage associated with poly-cytotoxic cytokine profiles[74]. Therefore, it is possible that within the context of adult influenza virus infection, γδ T cells could contribute to inflammation-mediated pathology rather than tissue repair.

The results presented in this study emphasize the need to evaluate anti-influenza virus responses and vaccine efficacy from both the serologic and cellular standpoint, and argue that composition of baseline cell populations is a better overall predictor of influenza susceptibility than serology and vaccine status alone. As baseline cellular and humoral immune landscapes vary significantly within human populations and across study cohorts, we propose that the protection-associated cell profiles defined in this study are a better metric to evaluate influenza susceptibility than any one cell population or serology measure. While individual cellular CoP against symptomatic influenza likely differ between cohorts, their individual functions may contribute to a converging protective immune profile, which can be more easily compared across studies. Further, the statistical and predictive models described here will also serve as useful tools to evaluate vaccine efficacy, identify new targets for next-generation vaccines promoting both cellular and humoral responses, and identify additional at-risk human populations for vaccination. However, further questions remain. It will be important for follow-up studies to validate these risk and protection models across more diverse cohorts to determine if there are population-specific baseline cell profiles correlated with vaccine failure or disease severity. Assessment of CMI and innate responses are especially important during pregnancy[75] and in adults above the age of 65 who are known to generate poor protective humoral responses following immunization[76,77]. The continuing aim of SHIVERS-II is to assess the immunological parameters of influenza virus infection and vaccination over several years. As the data presented in this study are derived from subjects enrolled in the inaugural year of the SHIVERS-II study, there is great potential for future studies using this cohort to validate and expand on these results for years to come.

STUDY LIMITATIONS

We acknowledge several limitations within our study. The first is the relatively small sample size across comparator groups and, due to the increased circulation of A(H1N1) virus that year, an overrepresentation of infections caused by A(H1N1) virus means that no strong strain-specific conclusions regarding influenza B or A(H3N2) influenza viruses can be drawn. Future studies using samples collected in subsequent years of the SHIVERS-II

cohort will focus on providing further validation to the models described here and expanding the analyses to include a wider range of influenza virus types and subtypes. Second, subjects enrolled in the SHIVERS-II cohort comprise a limited regional, age, and genetic scope and, therefore, specific interpretations of these data should be made solely within this context. Further validation of our risk modeling and associated cell profiles should be compared across a more diverse ethnogeographic space to account for the large degree of baseline variability across subjects. Finally, limited considerations were made regarding genetic contributions to risk of influenza, as while ethnicity was reported, this is not a robust evaluation of genetic background[78]. Despite these limitations, data presented here are from a subset of Year 1 participants and it is our directive to continue to investigate this important population across multiple years of the SHIVERS-II study.

METHODS

SHIVERS-II study design and participant definitions

The second iteration of the Southern Hemisphere Influenza Vaccine Efficacy Research and Surveillance (SHIVERS-II) study is a population-based, longitudinal (2018–2022) prospective cohort in Wellington, New Zealand initiated to evaluate cellular and serologic immune responses at baseline and during recall among adults with current influenza virus vaccination and/or infection. During year 1 (2018), more than 22,000 individuals aged 20–69 years were randomly selected for recruitment from 3 participating primary health organizations' healthy patient networks. Selected individuals received a study invitation and information packet by mail and those interested provided consent through an online electronic consent form and questionnaire in which demographic and contact information, vaccination and health and influenza-like illness status was provided. A total of 2,195 ultimately enrolled following written informed consent (Fig. 1a). Each participant provided one baseline blood draw (pre-season, usually during March-May) and another post-season blood draw (usually during October through December). Consented participants received NZ$30 gift card after each blood or swab sample collection to recognize their time and effort. Whole blood samples were collected in vacuum tubes containing heparin. Additional samples, including blood draws or nasal swabs, were required for participants with PCR-confirmed influenza virus infection or who received an influenza virus vaccination during the influenza season (May through September). Briefly, participants who received an influenza virus vaccine during this time provided a blood draw sample 14 days-post vaccination (post-vaccine baseline). All participants were monitored through weekly surveys for influenza-like illness (ILI), defined by the WHO as "acute respiratory illness with cough and a history of fever/measured fever of ≥ 38°C and illness onset within the past 10 days"[79]. If ILI presented, a respiratory specimen (nasopharyngeal or throat swab) was collected and subjected to molecular testing for respiratory viruses by PCR (see methods below). Participants with both ILI and an associated influenza-positive PCR result were categorized as symptomatic influenza virus infection cases and additional acute (1–2 weeks post-ILI onset) and convalescent (4–7 weeks post-ILI onset) blood draws were taken. Respiratory samples from these PCR-positive influenza cases were further processed to determine the influenza virus subtype (see methods below). Inhibiting antibody titers against hemagglutinin (HA) and neuraminidase (NA) were determined from baseline and

post-season serum samples by hemagglutination-inhibition (HAI) assay or neuraminidase inhibition enzyme-linked lectin assay (NAI-ELLA), respectively (see methods below). Total binding antibody titers against purified, full-length HA and NA were measured by ELISA (see methods below). HAI titers were used to detect cryptic influenza virus infection cases not identified by PCR. Briefly, cryptic influenza virus infections were defined by 1) the absence of an ILI-associated influenza-positive PCR result, and 2) one of the following seroconversion parameters: unvaccinated participants with a ≥ 4-fold increase in pre-season to post-season HAI titer, vaccinated participants with a ≥ 4-fold increase in post-vax to post-season HAI titer, or vaccinated participants with a ≥ 4-fold increase in pre-season to post-season HAI titer who did not seroconvert following vaccination (i.e. seroconversion cannot be accounted for by vaccination), with the second titer of at least 1:40 in all cases.

Participant categorization and selection

Participants were categorized based on 2018 influenza virus vaccination (vaccinated or unvaccinated), or infection (symptomatic or cryptic) status. The symptomatic influenza virus infection group met the WHO-defined criteria for ILI and had a positive influenza virus PCR test. Cryptic influenza virus infections were defined as reporting 0–1 mild symptom(s) that did not meet the WHO-defined ILI criteria (and therefore do not have an associated PCR test) but were confirmed to have had a cryptic influenza virus infection via seroconversion. All cryptic infections in this study are, by definition, subclinical as no influenza PCR-positive-associated ILI was reported. The uninfected group did not meet the WHO-defined ILI criteria, did not have an associated PCR test performed, and were negative for cryptic infection. A total of 206 participants were selected from year 1 of the SHIVERS-II study and comprised 82 males (39.8%) and 124 females (60.2%) residing in the Wellington, New Zealand catchment area, with an average age of 43.8 ± 12.6 years (range 20–68 years), body mass index (BMI) of 27.5 ± 5.6 kg/m^2 (range 18.3–48.5 kg/m^2), and who predominantly self-identified as New Zealand-European descent (83.0%; Table 1). Participants were selected into four comparator groups including vaccinated-uninfected (n=75), vaccinated-infected (n=33), unvaccinated-uninfected (n=76), and unvaccinated-infected (n=22). Subjects' age (in years) and sex (assigned at birth) were roughly matched when selecting across comparator groups. Sample size requirements for statistical testing of the covariates were calculated using the R package WMWssp v0.4.0[80–82] with a defined power of 0.8 and were determined to be sufficient in size for the planned comparisons.

Composition of 2018 influenza virus vaccination

The 2018 seasonal quadrivalent influenza virus vaccine contained the following four components i) A/Michigan/45/2015 (H1N1)pdm09-like virus; ii) A/Singapore/INFIMH-16-0019/2016 (H3N2)-like virus; iii) B/Phuket/3073/2013-like virus (B/Yamagata lineage); iv) B/Brisbane/60/2008-like virus (B/Victoria lineage).

Molecular testing for respiratory viruses

For detection of respiratory viruses including influenza viruses, the Centers for Disease Control and Prevention (CDC) standard real-time reverse transcriptase (RT) PCR assay was performed on RNA extracted from participant nasopharyngeal or throat swabs as previously

described[83–87]. All samples were tested for a standard panel including influenza A (subtypes of A/H1N1pdm09, A(H3N2)) viruses, influenza B (B/Yamagata and B/Victoria lineages) viruses, respiratory syncytial virus, rhinovirus, human metapneumovirus, parainfluenza types 1–3, adenovirus, and enterovirus.

Influenza virus antigenic typing

Infecting influenza virus strain antigen typing was performed on all samples identified as influenza virus-positive by qPCR with low cycle threshold (Ct) values. Following viral isolation by sample inoculation into Madin-Darby canine kidney cells stably expressing human α-2,6-sialyltransferase (MDCK-SIAT)[88] cells, antigenic typing for influenza viruses was performed using a HAI assay with standard antisera supplied by the WHO Collaborating Center in Melbourne, AU (WHOCC-Melbourne). Any un-typeable influenza A viruses were forwarded to WHOCC-Melbourne or at CDC-Atlanta for further characterization.

Hemagglutinin inhibition assay (HAI)

Anti-hemagglutinin antibody titers were determined by HAI assay as previously described for influenza A (A/Michigan/45/2015 (H1N1) pdm09-like; A/Singapore/INFIMH-16-0019/2016 (H3N2)-like) and influenza B (B/Brisbane/60/2008-like [B/Victoria lineage]; B/Phuket/3073/2013-like [B/Yamagata lineage]) viruses present in the 2018 SH vaccine and in regional circulation[38–40]. Briefly, serum samples were treated with receptor-destroying enzyme (Denka Seiken, Japan) at 37°C overnight, heat-inactivated at 56°C for 30 minutes and tested by HAI assay with 0.5% turkey red blood cells (RBCs). Serum was serially diluted two-fold in 96-well U-bottom plates beginning at a 1:10 dilution. 4 agglutinating doses were added to each well and incubated. Titers were read after 30 min incubation with 50 μL of 0.5% turkey RBCs.

Neuraminidase inhibition enzyme-linked lectin (ELLA) assay

Anti-neuraminidase inhibiting (NAI) antibody titers were determined by ELLA for influenza A and B virus[39,89,90]. Briefly, recombinant viruses, composed of the NA from each of the influenza A viruses used for HAI and a mismatched H6 on a PR8 backbone, were generated by reverse-genetics and used as antigen. Serum samples were tested at a starting dilution of 1:10. Because no recombinant antigen was available for influenza B viruses, ELLA was performed against the whole B/Brisbane/60/2008 virus (B/Victoria lineage), as was previously described[91].

Enzyme-linked immunosorbent assay (ELISA)

EIA/RIA 96 well plates (Corning #3590) were individually coated with 0.5 μg purified recombinant influenza virus HA or NA protein at 0.01 mg/mL. HA antigens derived from A/Michigan/45/2015 (representative H1, Sino Biological, #40567-V08H1), A/Singapore/INFIMH-16-0019/2016 (representative H3, Sino Biological, #40580-V08H), B/Phuket/3073/2013 (representative B/Yamagata Lineage, Sino Biological, #40498-V08B), or B/Brisbane/60/2008 (representative B/Victoria Lineage, Sino Biological, #40016-V08H) and NA antigens derived from A/Michigan/45/2015 (representative N1, Sino

Biological, #40568-V07H), A/Singapore/INFIMH-16-0019/2016) (representative N2, Sino Biological, #40802-V08B), B/Phuket/3073/2013 (representative B/Yamagata Lineage, Sino Biological, #40502-V07B), or B/Washington/02/2019 (representative B/Victoria Lineage, Sino Biological, #40790-V08B) were used. Coated plates were sealed and stored at 4°C for 24 h. Serum samples were RDE treated by adding 3x volume of receptor destroying enzyme (Accurate Chemical, #YCC340122) to 1x volume of sera and incubated at 37°C overnight. Sera was then heat treated at 56 °C for 1 h after which 6-times the volume of 1x PBS was added to obtain a 1:10 starting dilution of sera. Plates were washed 3 times with 1x PBS and coated with 100 μL/well of blocking buffer (1% BSA (Gibco, #15260037) and 0.01% Tween-20 (ThermoFisher, #85113) in 1x PBS) for 6 h at 25°C. RDE-treated serum samples were titrated 1:160-1:20480 in blocking buffer and 50 μL of each serum dilution or blocking buffer (negative control) was added to replicate wells following removal of blocking buffer. The plates were then sealed and incubated at 4°C overnight. Plates were washed 3 times with wash buffer (0.05% Tween-20 in 1x PBS), 100 μL of anti-Human IgG (Fab specific)-HRP secondary antibody (Sigma cat #A0293, polyclonal, lot# 0000201676, dilution 1:3000) was added to each well, and incubated at 4°C overnight. Plates were washed 3 times in wash buffer and 50 μL of tetramethylbenzidine (TMB; Sigma, #T0440) was added to each well. After 8 minutes, 50 μL/well of stop solution (1N H_2SO_4 (Sigma #T0440) was added and the plates were read at 450 nm on the BioTek Synergy H1 microplate reader. To normalize, average OD values from negative control wells were subtracted from the average OD of replicate sample wells per-plate. Area under curve (AUC) values were calculated from XY plots of dilution by normalized OD values in GraphPad Prism 9 (v9.5.1 (528)) using the following parameters: baseline y=0; minimum peak height <10% of the distance from min to max Y; all peaks above baseline; 5 significant digits.

Flow cytometry: surface and intracellular staining

Cryopreserved aliquots of PBMCs were thawed at 37°C, suspended in RPMI-1640 supplemented with 10% heat-inactivated FBS (Gibco, cat# 16140071), 1% non-essential amino acids (Gibco, cat# 11140-050), 1 mM sodium pyruvate (Gibco, cat# 11360-070), and 1% penicillin-streptomycin (10,000 U/mL penicillin and 10,000 μg/mL streptomycin; Gibco, cat# 15140-122). Cells were plated at $3.0–4.0\times10^5$ cells/well in a 96-well U-bottom plate.

For peptide stimulated PBMCs, pooled peptides (BEI Resources cat# NR-2667) derived from influenza virus matrix (M), nucleoprotein (NP), and polymerase basic 1 (PB1) protein were added to wells at a final concentration of 5 μg/mL. For virus stimulation, PBMCs were infected with H1N1pdm09 (A/Michigan/45/2015) or H3N2 (A/Singapore/INFIMH-16-019/2016) at a multiplicity of infection (MOI) = 4 in viral infection media (RPMI-1640 completed with 0.3% BSA, 0.225% $NaCO_3$, 1% penicillin-streptomycin (10,000 U/mL penicillin and 10,000 μg/mL streptomycin; Gibco), 1% L-glutamine (Gibco), and 1% vitamin solution (Gibco)). Cell Stimulation Cocktail (BioLegend, cat# 423302; eBioscience, cat# 00-4970-93) were added to positive control wells. Media alone was used in unstimulated wells. After addition, cells were incubated for 2 h (peptide; mock) or 12 h (virus; Stimulation Cocktail) at 37°C. Brefeldin A (BioLegend cat# 420601; BD, cat# 555029) and Monensin (BD Cat #554715) were then added along with anti-

CD107a fluorophore-conjugated antibodies where appropriate, and incubated at 37°C for an additional 6 hr. Cells were washed twice in FACS buffer (DPBS, 2% FBS, 1mM EDTA pH 8.0), and treated with human Fc-block (BioLegend cat# 422302) for 10 min at 4°C.

Cells were stained for 30 min at 4°C with the following antibodies/dyes: CCR3 AF647 (BioLegend cat# 310710, clone 5E8, lot# B312457, dilution 1:50), CCR5 PerCP/eFluor710 (ThermoFisher cat# 46-1951-82, clone 7A4, lot# 4324286, dilution 1:80), CCR7 PE/Cy7 (BioLegend cat# 353226, clone G04H7, lot# B305236, dilution 1:20), CD1c PE/Cy7 (BioLegend cat# 331516, clone L161, lot# B256006, dilution 1:20), CD3 BV750 (BioLegend cat# 344846, clone SK7, lot# B303395, dilution 1:200), CD3 BV510 (BioLegend cat# 300448, clone UCHT1, lot# B281774, dilution 1:200), CD4 BB515 (BD cat# 565996, clone SK3, lot# 9343297, dilution 1:200), CD8 BV570 (BioLegend cat# 301038, clone RPA-T8, lot# B281322, dilution 1:50), CD11b CD785 (BioLegend cat# 301346, clone ICRF44, lot# B315938, dilution 1:100), CD11c BV650 (BioLegend cat# 337238, clone Bu15, lot# B304739, dilution 1:20), CD14 APC/Fire750 (BioLegend cat# 367120, clone 63D3, lot# B257669, dilution 1:100), CD16 FITC (BioLegend cat# 360716, clone B73.1, lot# B300038, dilution 1:100), CD19 BV510 (BioLegend cat# 302242, clone HIB19, lot# B281769, dilution 1:200), CD33 PE (BioLegend cat# 303404, clone WM53, lot# B288411, dilution 1:20), CD40 AF700 (BioLegend cat# 334328, clone 5C3, lot# B272227, dilution 1:20), CD45RA V450 (ThermoFisher cat# 48-0458-42, clone HI100, lot# 2263338, dilution 1:200) or BV570 (BioLegend cat# 304132, clone HI100, lot# B319894, dilution 1:20), CD45RO APC/Fire 750 (BioLegend cat# 304250, clone UCHL1, lot# B288981, dilution 1:20), CD56 PE-Cy5 (BioLegend cat# 362516, clone 5.1H11, lot# B317268, dilution 1:100), CD64 BV711 (BD cat# 740782, clone 10.1, dilution 1:20), CD80 SuperBright 436 (ThermoFisher cat# 62-0809-42, clone 2D10.4, lot# E113289A, dilution 1:20), CD103 BV605 (BioLegend cat# 350217, clone Ber-ACT8, lot# B359323, dilution 1:20), CD107a BV711 (BioLegend cat# 328640, clone H4A3, lot# B301430, dilution 1:50) or PE/Dazzle 594 (BioLegend cat# 328646, clone H4A3, lot# B319152, dilution 1:20), CD123 PE (BioLegend cat# 306006, clone 6H6, lot# B269700, dilution 1:100) or PerCP/Cy5.5 (BioLegend cat# 306016, clone 6H6, lot# B318963, dilution 1:20), CD141 BV421 (BioLegend cat# 344144, clone M80, lot# B315574, dilution 1:100), CD177 APC (BioLegend cat# 315808, clone MEM-166, lot# B265153, dilution 1:50), CXCR3 PE/Dazzle594 (BioLegend cat# 353736, clone G025H7, lot# B289168, dilution 1:100) or BV711 (BioLegend cat# 353732, clone G025H7, lot# B264427, dilution 1:20), CXCR5 SuperBright436 (ThermoFisher cat# 62-9185-42, clone MU5HBEE, lot# 2279709, dilution 1:100), HLA-A2 BV650 (BioLegend cat# 343324, clone BB7.2, lot# B290341, dilution 1:200), HLA-DR AF700 (BioLegend cat# 307626, clone L243, lot# B272227, dilution 1:100) or PE/Dazzle 594 (BioLegend cat# 307654, clone L243, lot# B320167, dilution 1:20), ICOS PerCP/Cy5.5 (BioLegend cat# 313518, clone C398.4A, lot# B297477, dilution 1:20), GhostDye Violet 510 Viability Dye (Tonbo cat# 13-0870-T500, lot# D0870061322133, dilution 1:400), PD1 FITC (BioLegend cat# 329904, clone EH12.2H7, lot# B253784, dilution 1:100), Siglec-8 BV480 (BD cat# 747874, clone 837535, lot# 1006002, dilution 1:50), and TCRγδ AF647 (BioLegend cat# 331214, clone B1, lot# B274274, dilution 1:80).

Cells were washed twice with FACS buffer, then fixed and permeabilized using the Cytofix/CytoPerm Fixation and Permeabilization Kit (BD cat# 554714) according to the manufacturer's instructions. Cells were washed twice in Perm/Wash Buffer, then stained for 30 mins at 4°C with the following intracellular antibodies: CD68 PerCP/Cy5.5 (BioLegend cat# 333814, clone Y1/82A, lot# B273670, dilution 1:50), Granzyme B AF700 (BioLegend cat# 372222, clone QA16A02, lot# B321316, dilution 1:25), IL2 APC (ThermoFisher cat# 17-7029-82, clone MQ1-17H12, lot# 2172935, dilution 1:25), IL13 BV421 (BioLegend cat# 501916, clone JES10-5A2, lot# B319799, dilution 1:25), IL17 BV785 (BioLegend cat# 512338, clone BL168, lot# B310823, dilution 1:25), IL21 PE (BioLegend cat# 513004, clone 3A3-N2, lot# B299502, dilution 1:25), IFNγ BV480 (BD cat# 566100, clone B27, lot# 0261295, dilution 1:10), and TNFα BV605 (BioLegend cat# 502936, clone Mab11, lot# B312493, dilution 1:25). Cells were washed twice and resuspended in FACS buffer for flow cytometric analysis. Data were acquired on a Cytek 3-laser Aurora spectral flow cytometer using SpectroFlow v2.2 software (Cytek) and analyzed using FlowJo v10.7.1 (TreeStar). Spectral cytometry panels conform to best-practice principles in spectral analysis[92,93].

Flow cytometry: select cell subsets for primary analysis

Cell frequencies for more than 89 CMI and innate subtypes were resolved including populations previously shown to correlate with anti-influenza virus response. Several blinded quality control measures for unbiased selections were used to identify cell populations to include in primary analysis. These included filtering out individual samples with low cell viability (5% and below) and/or high cellular debris (>25% of events) and eliminating cell populations with a limited dynamic range in cell frequency. Using these measures, we reduced our individual myeloid populations from 23 to 16 and lymphoid cell populations from 66 to 41 for primary analyses. Please refer to Supplementary Table 7 for cell population naming conventions used in this study.

Defining co-regulated immune cell modules

Co-regulated immune cell modules were independently determined for myeloid or lymphoid cell populations across all vaccinated and unvaccinated participants. For the myeloid cell populations, modules ("Clusters") were identified by significant positive correlation between cell frequencies (% parent) using Pearson's bivariate correlation and a false discovery rate (FDR) adjustment cutoff of $q \leq 0.05$. To define modules within the lymphoid compartment, cell population frequencies (% parent) were first averaged across viral (MOI = 4, A/Michigan/45/2015 (H1N1)pdm09 or A/Singapore/INFIMH-16-019/2016 (H3N2)) and peptide (1–5 μM/peptide pools containing M1, NP, PB1) stimulation conditions to give the average stimulated cell frequency ('Stim Average'). Lymphoid Clusters were then identified by significant positive correlation between Stim Average frequencies using Pearson's bivariate correlation with FDR adjustment cutoff of $q \leq 0.05$. Analyses were performed using the base library in R v3.6.0[94].

Statistical modeling

Univariate statistical comparisons presented in Supplementary Table 3 were performed independently on vaccinated and unvaccinated subjects and presented as differences between cases (symptomatic influenza) and controls (uninfected and cryptic influenza) within each

group. Categorical variables and associated levels are displayed as counts and percentages across the target variable and Fisher's exact test was used to compute *p* values to test the significance of association of the variable across cases and controls. Continuous variables are represented by their median and interquartile range across symptomatic and cryptic/uninfected groups, and significance of difference across the two groups is computed using the single-sided Kruskal-Wallis test. Statistical analyses were performed using the base library in R v3.6.0[94] and sjTabone v0.1.0[95]. Six subjects with consistent cell frequency outliers across multiple cell populations determined by Grubbs' test ($p \leq 0.05$) were excluded for a total of 200 subjects analyzed.

Univariate regression modeling was performed individually on all cellular covariates for vaccinated and unvaccinated subjects separately, on selected co-regulated cell modules, and on a subset of cryptic and symptomatic infection participants for serology measures. Binomial regression models were built from each cellular or serology measure, or Cluster frequency (independent variable) to evaluate effects on symptomatic infection risk (dependent variable). Individual multivariate regression models describing risk of symptomatic influenza given individual serology measures adjusted for age (years), sex, BMI (kg/m^2), and 2018 vaccine status were also generated. Logit estimates from each GLM were transformed exponentially to give Odds Ratio values.

For the multivariate logistic regression considering demographic, vaccination status, serology, and cell immune measures, a stepwise approach was taken to identify appropriate variables to include in the GLM. First, we identified highly correlated cell population clusters for both lymphoid and myeloid compartments (Fig. 7b) or across serology measures (Extended data figure 2a). The resulting Pearson's correlation coefficients were informative in selecting representative immune measures from each cluster to be used in statistical models. Inhibiting titers for all HAI and NAI were log2-transformed. All serology measures and cell populations found to be influenced by vaccination status in the univariate analyses were considered as both individual covariates and as interacting terms with 2018 influenza vaccine status. As collinearity is a common problem in studies where the underlying phenomenon that generates the observations is not fully specified, we also assessed multicollinearity across all covariates by variance inflation factor (VIF) analysis. The results from the correlation and VIF analyses identified a 'selected' set of covariates that could be used in traditional regression methods without overfitting. A GLM was constructed with the final set of select covariates against a response variable denoting symptomatic infection status. Stepwise regression models (both forwards selection and backwards elimination) were also constructed using Akaike information criterion (AIC) as the metric of model effectiveness. The final stepwise model had a lower AIC compared to the select GLM but resulted in a higher residual deviance. Bayesian model averaging (BMA) was also used to test the strength of the selected covariates when averaged over a wider range of models. Continuous dependent covariates were normalized using scaled mean values and standard deviations (Age; ELISA AUC; % parent cell frequency) or by log2 transformation (HAI; NAI). Multivariate analyses were performed using the base library in R v3.6.0[94] and BMA v3.18.17[96].

Univariate protection and susceptibility thresholds

Receiver-operating characteristic (ROC) curves were used to test the effectiveness of each univariate immune measure–from all, vaccinated, and unvaccinated participant subsets – as a diagnostic[97,98]. From the ROC analysis we i) measured trade-offs between sensitivity and specificity of a given immune measure, and ii) determined the optimal threshold achieving 50% sensitivity to generalize the behavior of the measure. The area under the ROC curve (AUC) was also determined for each immune measure and indicates the overall quality of the measure in capturing true positives. Analyses were performed using the base library in R v3.6.0[94].

Predictive modeling

An 80:20 (train:test) split was performed on 200 participants (removal of six subjects with significant cell population frequency outliers) while ensuring equivalent proportions of cases (symptomatic influenza) and controls (uninfected and cryptic influenza). Four separate random forest models were built: (i) a Base model that predicts symptomatic infection using demographic (age; sex; BMI category; ethnicity; 2018 influenza virus vaccine status), and serologic (HAI A(H1); HAI A(H3); HAI B/Victoria (lineage); HAI B/Yamagata (lineage); NAI A(N1); NAI A(N2); NAI B/Victoria (lineage); NAI B/Yamagata (lineage); A(H1) AUC; A(H3) AUC; B/Victoria (lineage) HA AUC; B/Yamagata (lineage) HA AUC; A(N1) AUC; A(N2) AUC; B/Victoria (lineage) NA AUC; B/Yamagata (lineage) NA AUC covariates; (ii) a Lymphoid model that uses the variables from the Base model and cell populations from the lymphoid panel (CD4 Total; CD4 TNFα$^+$; CD4 Effector; CD4 IL-2$^+$; CD4 Naïve; CD4 PD1$^+$; CD4 Th17; CD4 dual producers; CD8 Total; CD8 CD107a$^+$; CD8 Effector; CD8 IFNγ$^+$; CD8 IL-2$^+$; CD8 Memory CCR5$^+$; CD8 PD1$^+$; CD8 TNFα$^+$; CD8 single-producers; CD8 dual-producers; cTfh CXCR3$^+$; cTfh ICOS$^+$; NK GzmB^{neg}IFNγ$^+$; NK GzmB$^+$IFNγ$^+$; NK GzmB$^+$IFNγ^{neg}; γδ T cells); (iii) a Myeloid model that uses the variables from the Base models and cell populations from the Myeloid panel (mDC; NK CK Producing; NK Activated; NK Cytotoxic; Monocytes Intermediate; Monocytes Nonclassical; Basophils; Eosinophils); (iv) a Combined model that uses all available variables; Myeloid Only model containing populations from the myeloid panel alone; (vi) Lymphoid Only model containing populations from the lymphoid panel alone; (vii) Lymphoid+Myeloid Model containing populations from both the lymphoid and myeloid panels. For cellular variables with high frequency correlation, a representative population was selected for inclusion into the models. 5-fold cross-validation was performed to avoid overfitting the data and was repeated 3 times to generate reliable metrics of model performance. Model performance was measured by sensitivity, specificity, and by scoring test-set data and plotting receiver-operating characteristic (ROC) curves. Variable of Importance (VIP) analysis was performed on the combined model and values were scaled between 0 and 100, with higher values denoting a higher impact on prediction. Random forest and VIP analyses were performed using the base library in R v3.6.0[94] and caret v6.0-92[99].

Data visualization

Data visualizations were performed in R v3.6.0 using ggplot2 v3.4.0[100], and ggpubr v0.5.0[101], and assembled using Adobe Illustrator 2023 software. Figure 1b was created

with BioRender.com and exported under a paid subscription with an associated publication license.

Extended Data

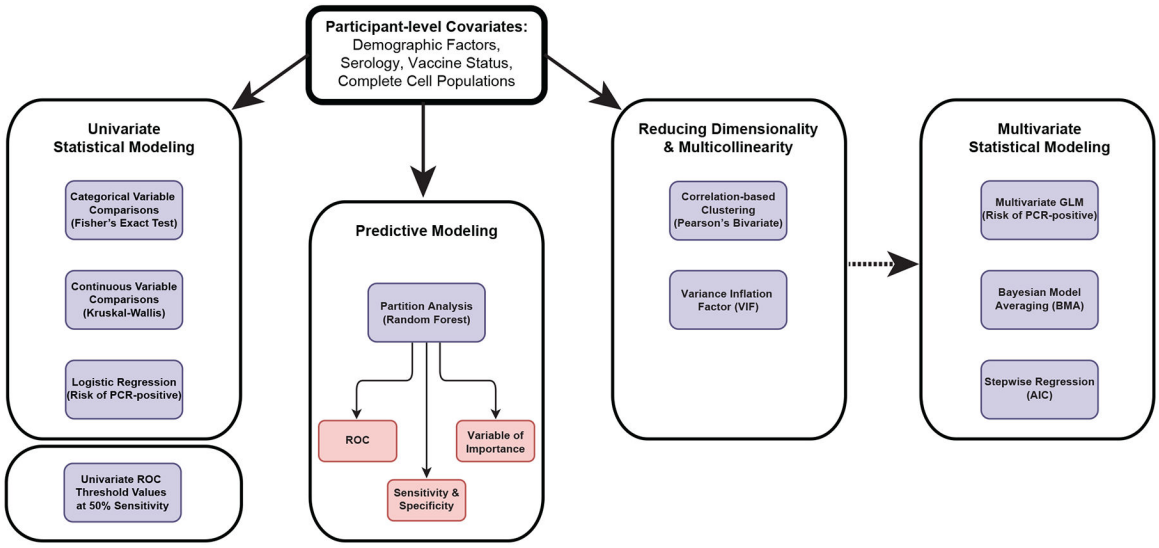

Extended Data Fig. 1.
Data analysis pipeline for predictive and statistical modeling

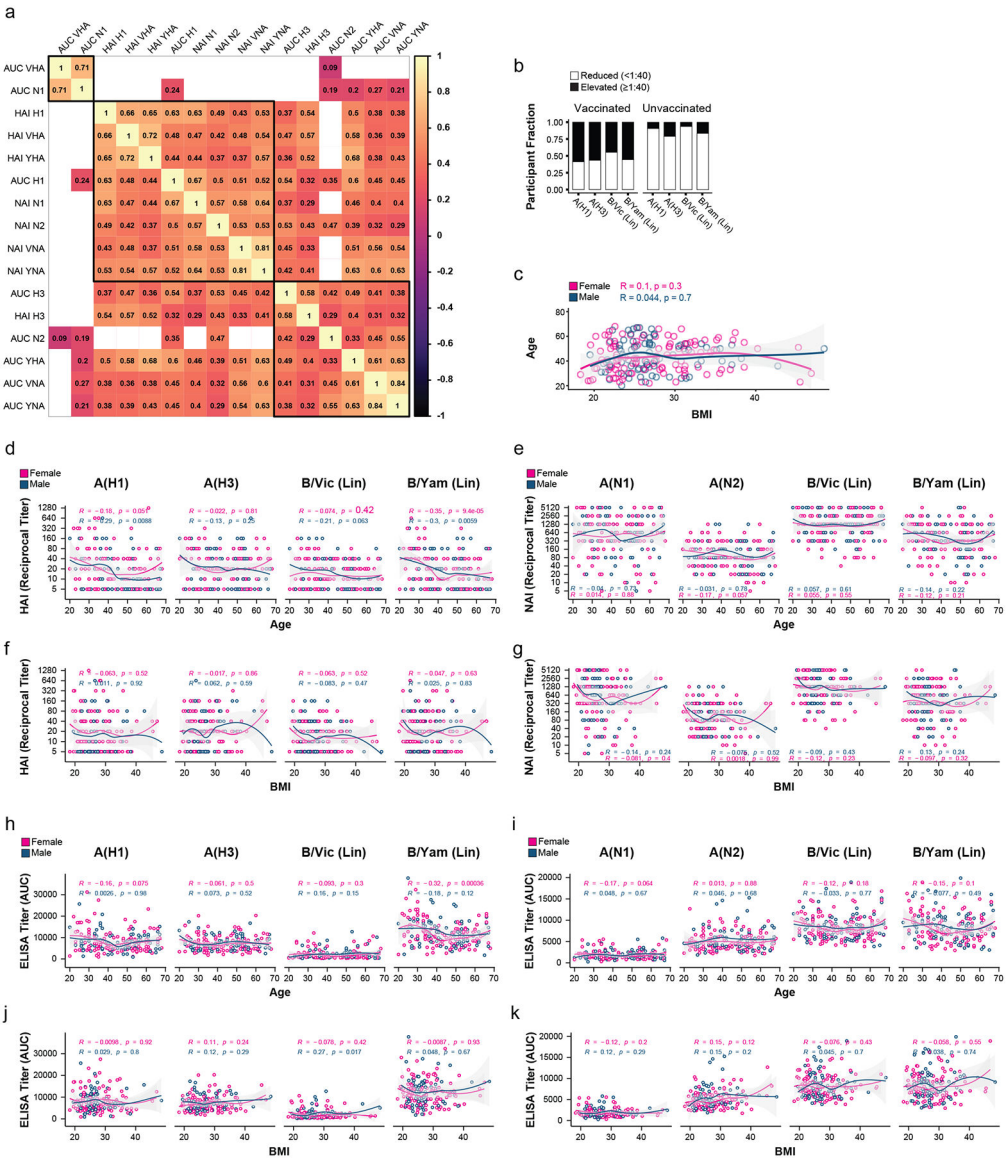

Extended Data Fig. 2:
Participant demographic and serologic correlations

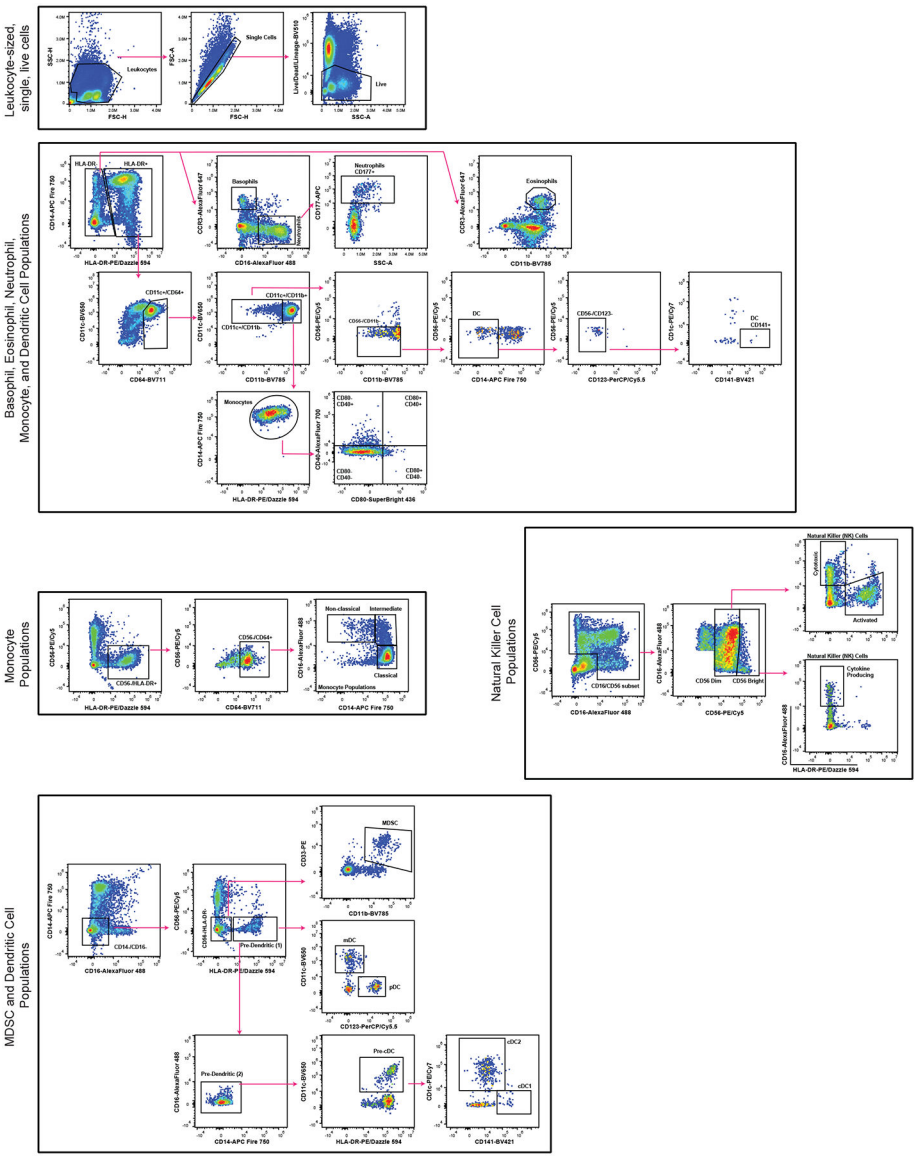

Extended Data Fig. 3:
Myeloid panel gating strategy

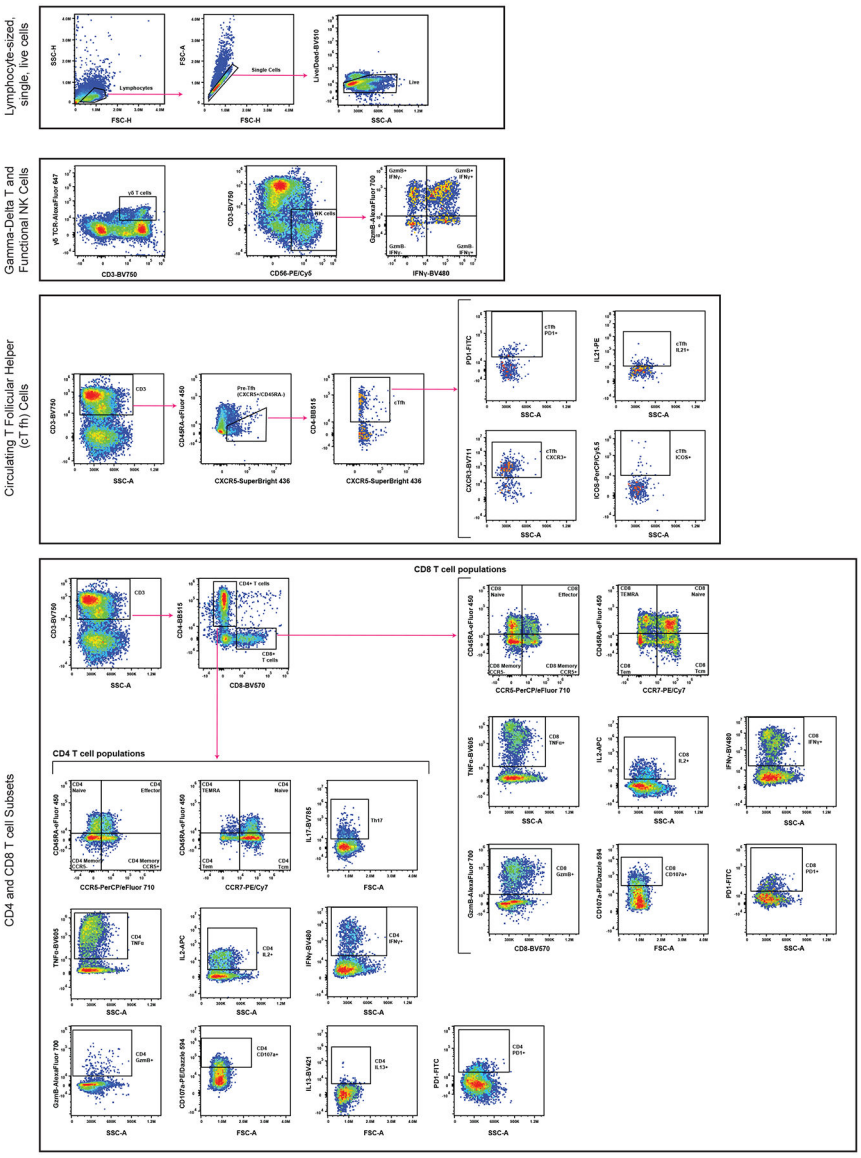

Extended Data Fig. 4.
Lymphoid and ICS panel gating strategy

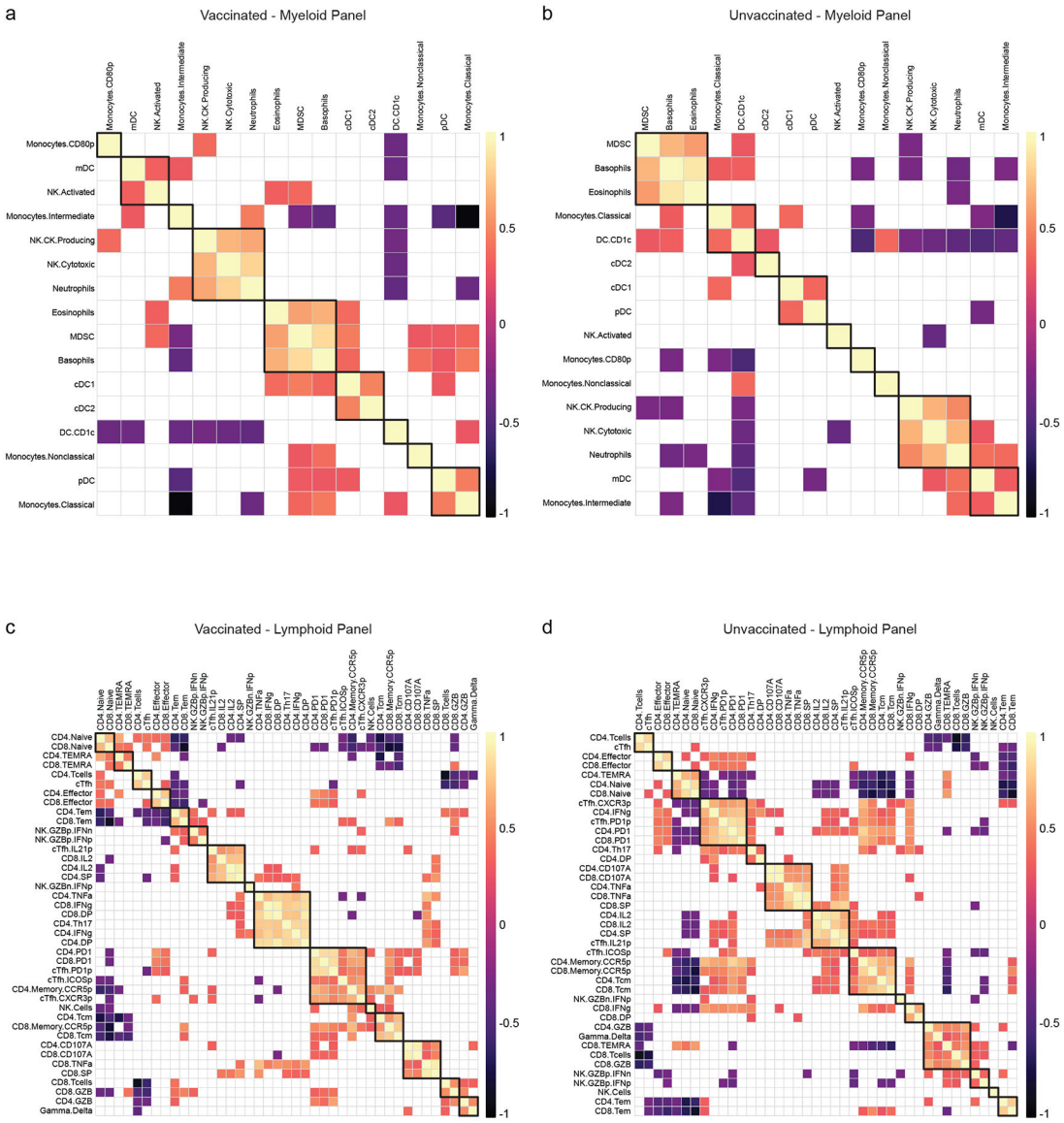

Extended Data Fig. 5:
Co-regulated immune cell clusters by vaccine status

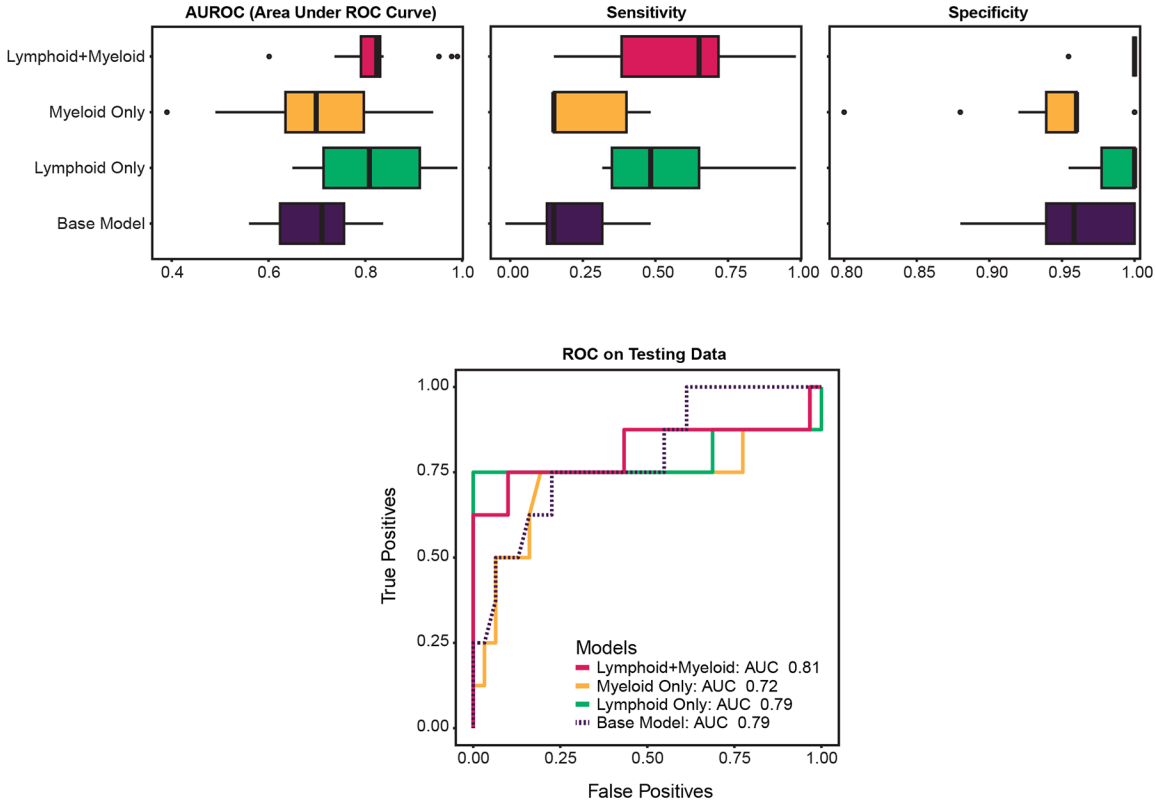

Extended Data Fig. 6:
Decision tree model comparison from cellular covariates

Supplementary Material

Refer to Web version on PubMed Central for supplementary material.

ACKNOWLEDGEMENTS

We thank Amanda DeCleene, Kate MacGregor, Marcia Gawith, and Maxine Mitchell for their work as RPH Study Nurses and all unnamed members of the SHIVERS-II team. We thank Dr. Tomer Hertz (Ben-Gurion University of the Negev) for insightful discussions and expert feedback on modeling methodology. We thank all consented enrollees and their families for participation and commitment to the SHIVERS-II study. This publication was supported by ALSAC at St. Jude Children's Research Hospital (SJCRH), the SJCRH Center of Excellence for Influenza Research and Surveillance (P.G.T., R.J.W., Q.S.H.) contract #HHSN272201400006C, HHS contract 75N93021C00016 for the St. Jude Centers of Excellence for Influenza Research and Response (SJ CEIRR), HHS contract 75N93019C00052 for the Center for Influenza Vaccine Research for High Risk Populations (CIVR-HRP) of the Collaborative Influenza Vaccine Innovation Centers, National Institute of Allergy and Infectious Diseases (NIAID) award 3U01AI144616-02S1 (P.G.T.), U01AI150747 (P.G.T.), R01AI154470 (P.G.T.), and Ruth L. Kirschstein National Research Service Award (NRSA) Individual Postdoctoral Fellowship (NRSA-NIAID) award number F32AI157296 (R.C.M.). The content of this article is solely the responsibility of the authors and does not necessarily represent the official views of the National Institutes of Health.

COMPETING INTERESTS

P.G.T. has consulted or received honorarium and/or travel support from Illumina, JNJ, Pfizer, and 10X. P.G.T. serves on the Scientific Advisory Board of ImmunoScape and CytoAgents. The remaining authors declare no competing interests.

DATA AVAILABILITY

The published article includes all datasets generated or analyzed as a part of this study. Individual Source Data are provided with associated figures (where appropriate) per the data sharing agreement stipulated under the Ruth L. Kirschstein National Research Service Award (NRSA) Individual Postdoctoral Fellowship (NRSA-NIAID) award number F32AI157296 (R.C.M). Raw flow cytometry source files can be made available upon reasonable request.

REFERENCES

1. CDC. Estimated Influenza Illnesses, Medical visits, Hospitalizations, and Deaths in the United States — 2017–2018 influenza season. Influenza (Flu) https://www.cdc.gov/flu/about/burden/2017–2018.htm#Table1 (2018).
2. Iuliano AD et al. Estimates of global seasonal influenza-associated respiratory mortality: a modelling study. The Lancet 391, 1285–1300 (2018).
3. Flannery B et al. Interim estimates of 2016–17 seasonal influenza vaccine effectiveness — United States, February 2017. Morb. Mortal. Wkly. Rep 66, 167–171 (2017).
4. Flannery B et al. Interim estimates of 2017–18 seasonal influenza vaccine effectiveness - United States, February 2018. Morb. Mortal. Wkly. Rep 67, 180–185 (2018).
5. Jackson ML et al. Influenza vaccine effectiveness in the United States during the 2015–2016 season. N. Engl. J. Med 377, 534–543 (2017). [PubMed: 28792867]
6. NCIRD. Estimated flu-related illnesses, medical visits, hospitalizations, and deaths in the United States — 2019–2020 flu season. CDC https://www.cdc.gov/flu/about/burden/2017-2018.htm (2021).
7. Zimmerman RK et al. 2014–2015 Influenza Vaccine Effectiveness in the United States by Vaccine Type. Clin. Infect. Dis. Off. Publ. Infect. Dis. Soc. Am 63, 1564–1573 (2016).
8. Erbelding EJ et al. A Universal Influenza Vaccine: The Strategic Plan for the National Institute of Allergy and Infectious Diseases. J. Infect. Dis 218, 347–354 (2018). [PubMed: 29506129]
9. The Centers of Excellence for Influenza Research and Response (NIAID-CEIRR) Network. https://www.ceirr-network.org/ (2022).
10. The Collaborative Influenza Vaccine Innovation Centers (NIAID-CIVICs) Network. https://www.niaidcivics.org/ (2022).
11. Morens DM, Taubenberger JK & Fauci AS Rethinking next-generation vaccines for coronaviruses, influenzaviruses, and other respiratory viruses. Cell Host Microbe 31, 146–157 (2023). [PubMed: 36634620]
12. Fourati S et al. Pan-vaccine analysis reveals innate immune endotypes predictive of antibody responses to vaccination. Nat. Immunol 2022 1–11 (2022) doi:10.1038/s41590-022-01329-5. [PubMed: 34789862]
13. Hagan T et al. Transcriptional atlas of the human immune response to 13 vaccines reveals a common predictor of vaccine-induced antibody responses. Nat. Immunol 1–11 (2022) doi:10.1038/s41590-022-01328-6. [PubMed: 34789862]
14. Liston A, Humblet-Baron S, Duffy D & Goris A Human immune diversity: from evolution to modernity. Nat. Immunol 2021 2212 22, 1479–1489 (2021). [PubMed: 34795445]
15. Tsang JS et al. Global analyses of human immune variation reveal baseline predictors of postvaccination responses. Cell 157, 499–513 (2014). [PubMed: 24725414]
16. Tsang JS et al. Improving Vaccine-Induced Immunity: Can Baseline Predict Outcome? Trends Immunol. 41, 457–465 (2020). [PubMed: 32340868]
17. Souquette A et al. Integrated Drivers of Basal and Acute Immunity in Diverse Human Populations. BioRxiv Prepr. Serv. Biol 2023.03.25.534227 (2023) doi:10.1101/2023.03.25.534227.
18. Gounder AP & Boon ACM Influenza Pathogenesis: The Effect of Host Factors on Severity of Disease. J. Immunol 202, 341–350 (2019). [PubMed: 30617115]

19. Mettelman RC & Thomas PG Human susceptibility to influenza infection and severe disease. Cold Spring Harb. Perspect. Med 11, (2021).
20. Brodin P et al. Variation in the human immune system is largely driven by non-heritable influences. Cell 160, 37–47 (2015). [PubMed: 25594173]
21. Carr EJ et al. The cellular composition of the human immune system is shaped by age and cohabitation. Nat. Immunol 17, 461–468 (2016). [PubMed: 26878114]
22. Lakshmikanth T et al. Human Immune System Variation during 1 Year. Cell Rep. 32, 107923 (2020). [PubMed: 32697987]
23. Lee MN et al. Common Genetic Variants Modulate Pathogen-Sensing Responses in Human Dendritic Cells. Science 343, 1246980 (2014).
24. Mettelman RC, Allen EK & Thomas PG Mucosal immune responses to infection and vaccination in the respiratory tract. Immunity 55, 749–780 (2022). [PubMed: 35545027]
25. O'Neill MB et al. Single-Cell and Bulk RNA-Sequencing Reveal Differences in Monocyte Susceptibility to Influenza A Virus Infection Between Africans and Europeans. Front. Immunol 12, 768189 (2021). [PubMed: 34912340]
26. Orrù V et al. Genetic variants regulating immune cell levels in health and disease. Cell 155, 242–256 (2013). [PubMed: 24074872]
27. Patin E et al. Natural variation in the parameters of innate immune cells is preferentially driven by genetic factors. Nat. Immunol 19, 645 (2018).
28. Raj T et al. Polarization of the Effects of Autoimmune and Neurodegenerative Risk Alleles in Leukocytes. Science 344, 519–523 (2014). [PubMed: 24786080]
29. Randolph HE et al. Genetic ancestry effects on the response to viral infection are pervasive but cell type specific. Science 374, 1127–1133 (2021). [PubMed: 34822289]
30. Roederer M et al. The genetic architecture of the human immune system: a bioresource for autoimmunity and disease pathogenesis. Cell 161, 387–403 (2015). [PubMed: 25772697]
31. Ye CJ et al. Intersection of population variation and autoimmunity genetics in human T cell activation. Science 345, 1254665 (2014).
32. Cox RJ Correlates of protection to influenza virus, where do we go from here? Hum. Vaccines Immunother 9, 405 (2013).
33. Guthmiller JJ et al. First exposure to the pandemic H1N1 virus induced broadly neutralizing antibodies targeting hemagglutinin head epitopes. Sci. Transl. Med 13, eabg4535 (2021). [PubMed: 34078743]
34. Memoli MJ et al. Evaluation of antihemagglutinin and antineuraminidase antibodies as correlates of protection in an influenza A/H1N1 virus healthy human challenge model. mBio 7, (2016).
35. Monto AS et al. Antibody to influenza virus neuraminidase: An independent correlate of protection. J. Infect. Dis 212, 1191–1199 (2015). [PubMed: 25858957]
36. Ng S et al. Novel correlates of protection against pandemic H1N1 influenza A virus infection. Nat. Med (2019) doi:10.1038/s41591-019-0463-x.
37. Steel J et al. Influenza Virus Vaccine Based on the Conserved Hemagglutinin Stalk Domain. mBio 1, e00018–10 (2010). [PubMed: 20689752]
38. Bandaranayake D et al. Risk Factors and Immunity in a Nationally Representative Population following the 2009 Influenza A(H1N1) Pandemic. PLoS ONE 5, e13211 (2010). [PubMed: 20976224]
39. Huang QS et al. Risk Factors and Attack Rates of Seasonal Influenza Infection: Results of the Southern Hemisphere Influenza and Vaccine Effectiveness Research and Surveillance (SHIVERS) Seroepidemiologic Cohort Study. J. Infect. Dis 219, 347–357 (2019). [PubMed: 30016464]
40. Institute of Environmental Science and Research (ESR). 2018 Annual Influenza Summary. ESR Public Health Surveill. (2018).
41. Honce R & Schultz-Cherry S Impact of obesity on influenza A virus pathogenesis, immune response, and evolution. Front. Immunol 10, (2019).
42. Ursin RL & Klein SL Sex Differences in Respiratory Viral Pathogenesis and Treatments. Httpsdoiorg101146annurev-Virol.–091919–092720 8, 393–414 (2021).

43. Wu Y, Goplen NP & Sun J Aging and respiratory viral infection: from acute morbidity to chronic sequelae. Cell Biosci. 11, (2021).
44. Institute of Environmental Science and Research (ESR). 2017 Annual Influenza Summary. ESR Public Health Surveill. (2017).
45. Dormann CF et al. Collinearity: a review of methods to deal with it and a simulation study evaluating their performance. Ecography 36, 27–46 (2013).
46. Hamada H et al. Tc17, a Unique Subset of CD8 T Cells That Can Protect against Lethal Influenza Challenge. J. Immunol 182, 3469–3481 (2009). [PubMed: 19265125]
47. Annunziato F et al. Phenotypic and functional features of human Th17 cells. J. Exp. Med 204, 1849 (2007). [PubMed: 17635957]
48. Takagi R et al. B Cell Chemoattractant CXCL13 Is Preferentially Expressed by Human Th17 Cell Clones. J. Immunol 181, 186–189 (2008). [PubMed: 18566383]
49. Wang X et al. A critical role of IL-17 in modulating the B-cell response during H5N1 influenza virus infection. Cell. Mol. Immunol 8, 462–468 (2011). [PubMed: 21946434]
50. Bao J et al. Decreased frequencies of Th17 and Tc17 cells in patients infected with avian influenza A (H7N9) virus. J. Immunol. Res 2019, (2019).
51. Schultz-Cherry S Role of NK cells in influenza infection. Curr. Top. Microbiol. Immunol 386, 109–120 (2015). [PubMed: 24992894]
52. Riese P et al. Responsiveness to Influenza Vaccination Correlates with NKG2C-Expression on NK Cells. Vaccines 8, 1–18 (2020).
53. Jost S et al. Changes in cytokine levels and NK cell activation associated with influenza. PLoS ONE 6, (2011).
54. Björkström NK, Ljunggren H-G & Sandberg JK CD56 negative NK cells: origin, function, and role in chronic viral disease. Trends Immunol. 31, 401–406 (2010). [PubMed: 20829113]
55. Fox A et al. Severe pandemic H1N1 2009 infection is associated with transient NK and T deficiency and aberrant CD8 responses. PLoS ONE 7, (2012).
56. Heltzer ML et al. Immune dysregulation in severe influenza. J. Leukoc. Biol 85, 1036–1043 (2009). [PubMed: 19276177]
57. Bongen E, Vallania F, Utz PJ & Khatri P KLRD1-expressing natural killer cells predict influenza susceptibility. Genome Med. 10, 45 (2018). [PubMed: 29898768]
58. Dou Y et al. Influenza Vaccine Induces Intracellular Immune Memory of Human NK Cells. PLoS ONE 10, (2015).
59. Kay AW et al. Enhanced natural killer-cell and T-cell responses to influenza A virus during pregnancy. Proc. Natl. Acad. Sci. U. S. A 111, 14506–14511 (2014). [PubMed: 25246558]
60. Giurgea LT, Morens DM, Taubenberger JK & Memoli MJ Influenza Neuraminidase: A Neglected Protein and Its Potential for a Better Influenza Vaccine. Vaccines 8, 409 (2020). [PubMed: 32718039]
61. Rajendran M, Krammer F & McMahon M The Human Antibody Response to the Influenza Virus Neuraminidase Following Infection or Vaccination. Vaccines 9, 846 (2021). [PubMed: 34451971]
62. Wohlbold TJ et al. Vaccination with Adjuvanted Recombinant Neuraminidase Induces Broad Heterologous, but Not Heterosubtypic, Cross-Protection against Influenza Virus Infection in Mice. mBio 6, e02556–14 (2015). [PubMed: 25759506]
63. Turner JS et al. Human germinal centres engage memory and naive B cells after influenza vaccination. Nat. 2020 5867827 586, 127–132 (2020).
64. Bentebibel SE et al. Induction of ICOS+CXCR3+CXCR5+ T H cells correlates with antibody responses to influenza vaccination. Sci. Transl. Med 5, 176ra32 (2013).
65. Bentebibel SE et al. ICOS+PD-1+CXCR3+ T follicular helper cells contribute to the generation of high-avidity antibodies following influenza vaccination. Sci. Rep 6, 26494 (2016). [PubMed: 27231124]
66. Lindgren G et al. Induction of Robust B Cell Responses after Influenza mRNA Vaccination Is Accompanied by Circulating Hemagglutinin-Specific ICOS+ PD-1+ CXCR3+ T Follicular Helper Cells. Front. Immunol 8, (2017).

67. Currenti J et al. Tracking of activated cTfh cells following sequential influenza vaccinations reveals transcriptional profile of clonotypes driving a vaccine-induced immune response. Front. Immunol 14, (2023).
68. Pizzolla A et al. Influenza-specific lung-resident memory t cells are proliferative and polyfunctional and maintain diverse TCR profiles. J. Clin. Invest 128, 721–733 (2018). [PubMed: 29309047]
69. Lorenzo-Herrero S, Sordo-Bahamonde C, Gonzalez S & López-Soto A CD107a Degranulation Assay to Evaluate Immune Cell Antitumor Activity. in Cancer Immunosurveillance: Methods and Protocols (eds. López-Soto A & Folgueras AR) 119–130 (Springer, 2019). doi:10.1007/978-1-4939-8885-3_7.
70. Wilkinson TM et al. Preexisting influenza-specific CD4 + T cells correlate with disease protection against influenza challenge in humans. Nat. Med 18, 274–280 (2012). [PubMed: 22286307]
71. Krammer F The human antibody response to influenza A virus infection and vaccination. Nat. Rev. Immunol 19, 383–397 (2019). [PubMed: 30837674]
72. Guo XJ et al. Lung γδ T Cells Mediate Protective Responses during Neonatal Influenza Infection that Are Associated with Type 2 Immunity. Immunity 49, 531–544.e6 (2018). [PubMed: 30170813]
73. Clark BL & Thomas PG A Cell for the Ages: Human γδ T Cells across the Lifespan. Int. J. Mol. Sci 21, 1–18 (2020).
74. Sant S et al. Human γδ T-cell receptor repertoire is shaped by influenza viruses, age and tissue compartmentalisation. Clin. Transl. Immunol 8, e1079 (2019).
75. Savic M et al. Distinct T and NK cell populations may serve as immune correlates of protection against symptomatic pandemic influenza A(H1N1) virus infection during pregnancy. PLOS ONE 12, e0188055 (2017).
76. McElhaney JE et al. T Cell Responses Are Better Correlates of Vaccine Protection in the Elderly. J. Immunol 176, 6333–6339 (2006). [PubMed: 16670345]
77. McElhaney JE et al. Granzyme B: Correlates with protection and enhanced CTL response to influenza vaccination in older adults. Vaccine 27, 2418–2425 (2009). [PubMed: 19368783]
78. Mersha TB & Abebe T Self-reported race/ethnicity in the age of genomic research: its potential impact on understanding health disparities. Hum. Genomics 9, 1 (2015). [PubMed: 25563503]
79. WHO. Global Epidemiological Surveillance Standards for Influenza. 1–5 (2013).
80. Brunner E, Bathke AC & Konietschke F Rank and Pseudo-Rank Procedures for Independent Observations in Factorial Designs. (2018) doi:10.1007/978-3-030-02914-2.
81. Bürkner PC, Doebler P & Holling H Optimal design of the Wilcoxon–Mann–Whitney-test. Biom. J 59, 25–40 (2017). [PubMed: 27243898]
82. Happ M, Bathke AC & Brunner E Optimal sample size planning for the Wilcoxon-Mann-Whitney test. Stat. Med 38, 363 (2019). [PubMed: 30298671]
83. Huang QS et al. Implementing hospital-based surveillance for severe acute respiratory infections caused by influenza and other respiratory pathogens in New Zealand. West. Pac. Surveill. Response J. WPSAR 5, 23–30 (2014).
84. Kim C et al. Comparison of Nasopharyngeal and Oropharyngeal Swabs for the Diagnosis of Eight Respiratory Viruses by Real-Time Reverse Transcription-PCR Assays. PLOS ONE 6, e21610 (2011). [PubMed: 21738731]
85. Kodani M et al. Application of TaqMan low-density arrays for simultaneous detection of multiple respiratory pathogens. J. Clin. Microbiol 49, 2175–2182 (2011). [PubMed: 21471348]
86. Olsen SJ et al. Incidence of respiratory pathogens in persons hospitalized with pneumonia in two provinces in Thailand. Epidemiol. Infect 138, 1811–1822 (2010). [PubMed: 20353622]
87. Shu B et al. Design and performance of the CDC real-time reverse transcriptase PCR swine flu panel for detection of 2009 A (H1N1) pandemic influenza virus. J. Clin. Microbiol 49, 2614–2619 (2011). [PubMed: 21593260]
88. Matrosovich M, Matrosovich T, Carr J, Roberts NA & Klenk H-D Overexpression of the α-2,6-Sialyltransferase in MDCK Cells Increases Influenza Virus Sensitivity to Neuraminidase Inhibitors. J. Virol 77, 8418–8425 (2003). [PubMed: 12857911]

89. Sandbulte MR et al. Cross-reactive neuraminidase antibodies afford partial protection against H5N1 in mice and are present in unexposed humans. PLoS Med 4, e59 (2007). [PubMed: 17298168]

90. Wong SS et al. H5N1 influenza vaccine induces a less robust neutralizing antibody response than seasonal trivalent and H7N9 influenza vaccines. Npj Vaccines 2017 21 2, 1–8 (2017). [PubMed: 29263862]

91. Couzens L et al. An optimized enzyme-linked lectin assay to measure influenza A virus neuraminidase inhibition antibody titers in human sera. J Virol Methods 210C, 7–14 (2014).

92. Ferrer-Font L et al. Panel Design and Optimization for High-Dimensional Immunophenotyping Assays Using Spectral Flow Cytometry. Curr. Protoc. Cytom 92, 784884 (2020).

93. Liechti T et al. An updated guide for the perplexed: cytometry in the high-dimensional era. Nat. Immunol 1–8 (2021) doi:10.1038/s41590-021-01006-z. [PubMed: 33335328]

94. R Core Team. R: The R Project for Statistical Computing. https://www.r-project.org/ (2018).

95. Vegesana K sjTabone. (2023).

96. Raftery A, Hoeting J, Volinsky C, Painter I & Yeung KY BMA: Bayesian Model Averaging. (2022).

97. Mandrekar JN Receiver operating characteristic curve in diagnostic test assessment. J. Thorac. Oncol. Off. Publ. Int. Assoc. Study Lung Cancer 5, 1315–1316 (2010).

98. Greiner M, Pfeiffer D & Smith RD Principles and practical application of the receiver-operating characteristic analysis for diagnostic tests. Prev. Vet. Med 45, 23–41 (2000). [PubMed: 10802332]

99. Max K et al. Classification and Regression Training. 198 (2016).

100. Wickham H ggplot2. (Springer, 2009). doi:10.1007/978-0-387-98141-3.

101. Kassambara A ggpubr: ‘ggplot2’ Based Publication Ready Plots. (2022).

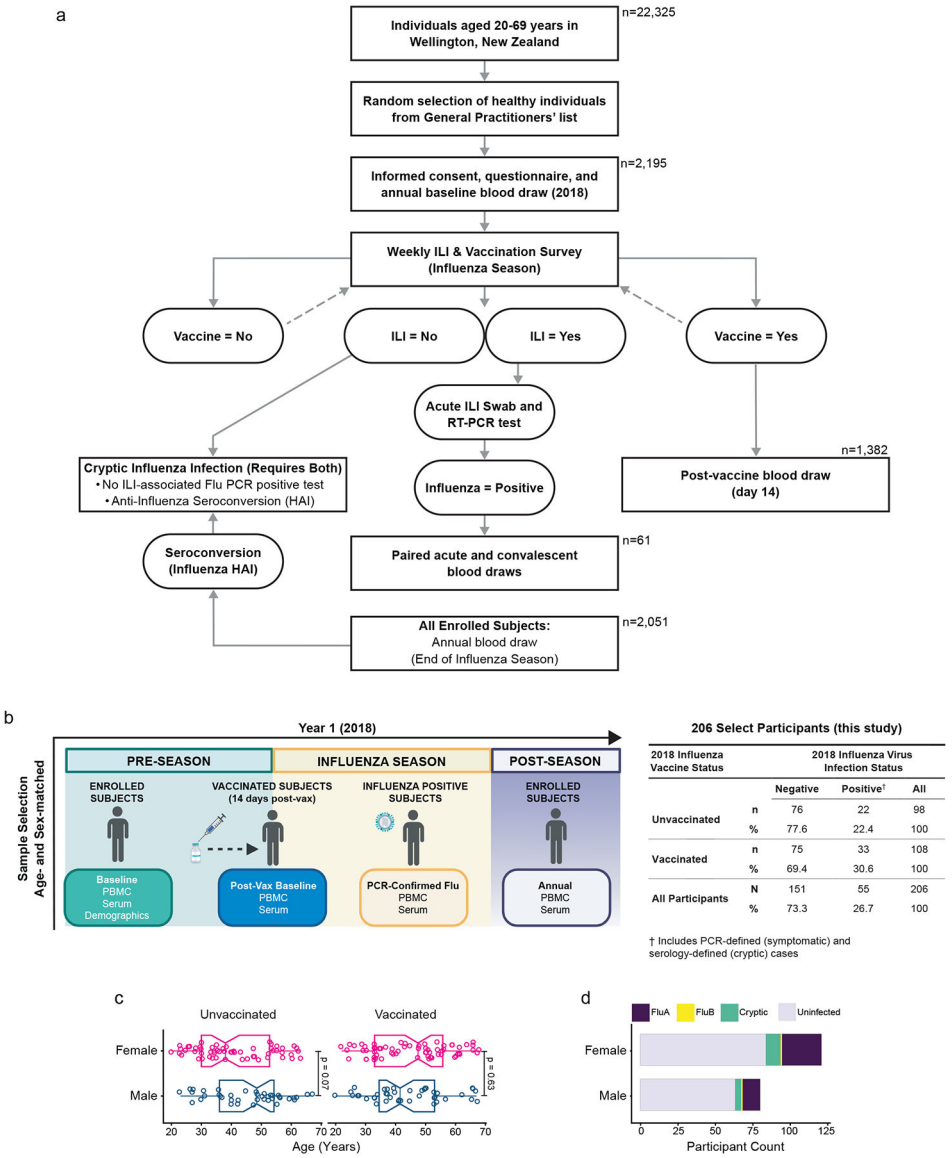

Figure 1: SHIVERS-II study design, subject enrollment, sample collection, and demographics.

a) Schematic depiction of the Southern Hemisphere Influenza and Vaccine Effectiveness Research and Surveillance 2 (SHIVERS-II) study design and participant numbers for Year 1 (2018). **b)** Following consented enrollment, demographic information and whole blood draws were collected from all vaccinated and unvaccinated subjects pre-season (non-vaccinated baseline) and 14 days post-vaccination (vaccinated baseline). Subjects meeting WHO-defined criteria for influenza-like illness (ILI) were tested for influenza viruses by PCR and confirmed cases were sampled further during acute infection. All enrolled subjects were sampled post-season. Cryptic infections were adjudicated post-season from ILI- and PCR-negative participants with a 4-fold or greater increase in HAI antibody titers without post-vaccination HAI seroconversion. (Right) 206 enrolled subjects were selected for study inclusion from four baseline comparator groups (unvaccinated-uninfected; unvaccinated-infected; vaccinated-uninfected; vaccinated-infected) based on age- and sex-

matching. **c)** Sex (assigned at birth) of n=206 participants stratified by vaccine status and age (years) compared by two-sided Wilcoxon rank sum test (unvaccinated-female (n=58) vs. unvaccinated-male (n=42) p= 0.07; vaccinated-female (n=66) vs. vaccinated-male (n=42) p= 0.63). Boxes represent the median and 25th to 75th percentiles; whiskers indicate the minimum (left) and maximum (right) values no further than 1.5 times the interquartile (IQR); notches extend 1.58*IQR / sqrt(n) providing 95% CI. P< 0.05 achieving significance. **d)** Participant sex stratified by influenza virus infection status and strain. Influenza A (FluA) virus category includes A(H1N1) and A(H3N2); influenza B (FluB) viruses include B/Victoria (lineage) and B/Yamagata (lineage) strains. PBMC (peripheral blood mononuclear cells).

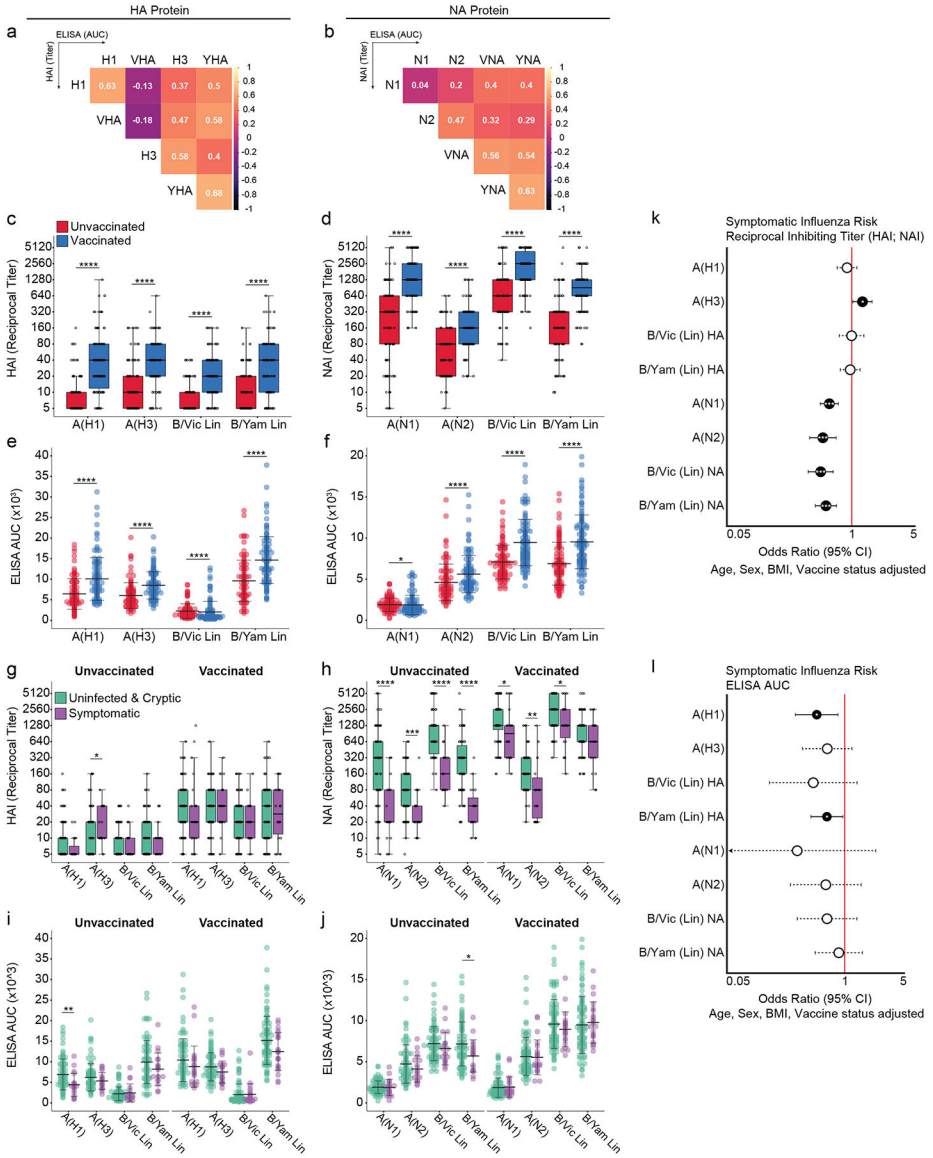

Figure 2: Individual serology measures correlate with protection from symptomatic influenza disease.

a-b) Spearman Rank correlations between **(a)** anti-HA (HAI; ELISA) or **(b)** anti-NA (NAI; ELISA) serology measures. **c-f)** Serology measures against **(c,e)** HA and **(d,f)** NA by influenza virus source comparing vaccinated (n=108) to unvaccinated (n=98) participants by two-sided Wilcoxon rank sum test. For **(c)** A(H1) $p< 2\times10^{-16}$, A(H3) $p= 4.5\times10^{-11}$, B/Vic (lin) $p= 1.6\times10^{-15}$, B/Yam (lin) $p= 4.1\times10^{-12}$; for **(d)** A(N1) $p< 2\times10^{-16}$, A(N2) $p= 1.5\times10^{-8}$, B/Vic (lin) $p= 6\times10^{-12}$, B/Yam (lin) $p= 9.4\times10^{-16}$; for **(e)** A(H1) $p= 5.3\times10^{-9}$, A(H3) $p= 2\times10^{-9}$, B/Vic (lin) $p= 4.5\times10^{-5}$, B/Yam (lin) $p= 4.8\times10^{-11}$; for **(f)** A(N1) $p= 0.033$, A(N2) p= 7.4×10^{-5}, B/Vic (lin) $p= 9.7\times10^{-11}$, B/Yam (lin) $p= 1.1\times10^{-9}$. **g-j)** Serology measures of vaccinated and unvaccinated participants against **(g,i)** HA and **(h,j)** NA by influenza virus source comparing uninfected and cryptic (n=165) to symptomatic (n=41) influenza virus infection using two-sided Wilcoxon rank sum test. For **(g)** unvaccinated: A(H1) $p= 0.280$, A(H3) $p= 0.024$, B/Vic (lin) $p= 1.0$, B/Yam (lin)

p= 0.922; vaccinated A(H1) p= 0.32, A(H3) p= 0.57, B/Vic (lin) p= 0.33, B/Yam (lin) p= 0.65; for **(h)** unvaccinated: A(N1) p= 1.6×10^{-6}, A(N2) p= 3.8×10^{-4}, B/Vic (lin) p= 4.4×10^{-7}, B/Yam (lin) p= 2.7×10^{-8}; vaccinated A(N1) p= 0.012, A(N2) p= 0.0013, B/Vic (lin) p= 0.033, B/Yam (lin) p= 0.212; for **(i)** unvaccinated: A(H1) p= 0.0037, A(H3) p= 0.450, B/Vic (lin) p= 0.713, B/Yam (lin) p= 0.239; vaccinated A(H1) p= 0.103, A(H3) p= 0.155, B/Vic (lin) p= 0.646, B/Yam (lin) p= 0.053; for **(j)** unvaccinated: A(N1) p= 0.781, A(N2) p= 0.393, B/Vic (lin) p= 0.161, B/Yam (lin) p= 0.028; vaccinated A(N1) p= 0.90, A(N2) p= 0.95, B/Vic (lin) p= 0.40, B/Yam (lin) p= 0.48. Boxes represent the median and 25th to 75th percentiles; whiskers indicate the minimum and maximum values no further than 1.5 times the interquartile (IQR); dot plots presented as mean± SD. Inhibiting titers presented as reciprocal endpoint dilutions calculated from HAI or NAI assays using A(H1N1), A(H3N2), B/Victoria (lineage), and B/Yamagata (lineage) viruses. Total binding antibody titers reported as AUC values calculated from ELISA assay against purified, full-length HA or NA proteins derived from influenza A(H1N1), A(H3N2), B/Victoria (lineage), and B/Yamagata (lineage) viruses. Means compared using two-sided Wilcoxon rank sum test. **k-l)** Relative risk of symptomatic infection among all participants (n=206) given individual anti-HA and anti-NA serology measures by **(k)** HAI and NAI, or **(l)** ELISA adjusted for participant age (years), sex, BMI (kg/m^2), and influenza vaccine status (2018) from individual GLMs. Odds Ratio (OR; center circle) with 95% CI (bars) derived from exponential transformation of GLM estimate (logit) values. HAI and NAI reciprocal inhibition endpoint values depicted at 1=log2 interval; ELISA AUC values depicted at 1=5000 interval. Positive effects on symptomatic influenza have OR > 1 while negative effects have OR < 1. Individual HAI or NAI models generated from 185 degrees of freedom (DOF) (symptomatic n=35, uninfected/cryptic n=151) except A(H3) HAI and B/Vic (lin) HAI (DOF = 184; symptomatic n=35, uninfected/cryptic n=150). Significance determined from GLM Pr(>|z|) output where z=estimate/SE. Resulting two-tailed p values: A(H1) HAI p= 0.368, A(H3) HAI p= 0.033, B/Vic (lin) HAI p= 0.983, B/Yam (lin) HAI p= 0.775, A(N1) NAI p= 2.4×10^{-6}, A(N2) NAI p= 3.0×10^{-5}, B/Vic (lin) NAI p= 1.9×10^{-6}, B/Yam (lin) NAI p= 4.1×10^{-6}. Individual HA and NA ELISA models generated from 187 DOF (symptomatic n=35, uninfected/cryptic n=153); Significance determined from GLM Pr(>|z|) output where z=estimate/SE. Resulting two-tailed p values: A(H1) AUC p= 0.011, A(H3) AUC p= 0.172, B/Vic (lin) AUC p= 0.163, B/Yam (lin) AUC p= 0.033, A(N1) AUC p= 0.232, A(N2) AUC p= 0.3, B/Vic (lin) AUC p= 0.252, B/Yam (lin) AUC p= 0.63. Not significant (blank); * $p\leq$ 0.05; ** $p\leq$ 0.01; *** $p\leq$ 0.001.

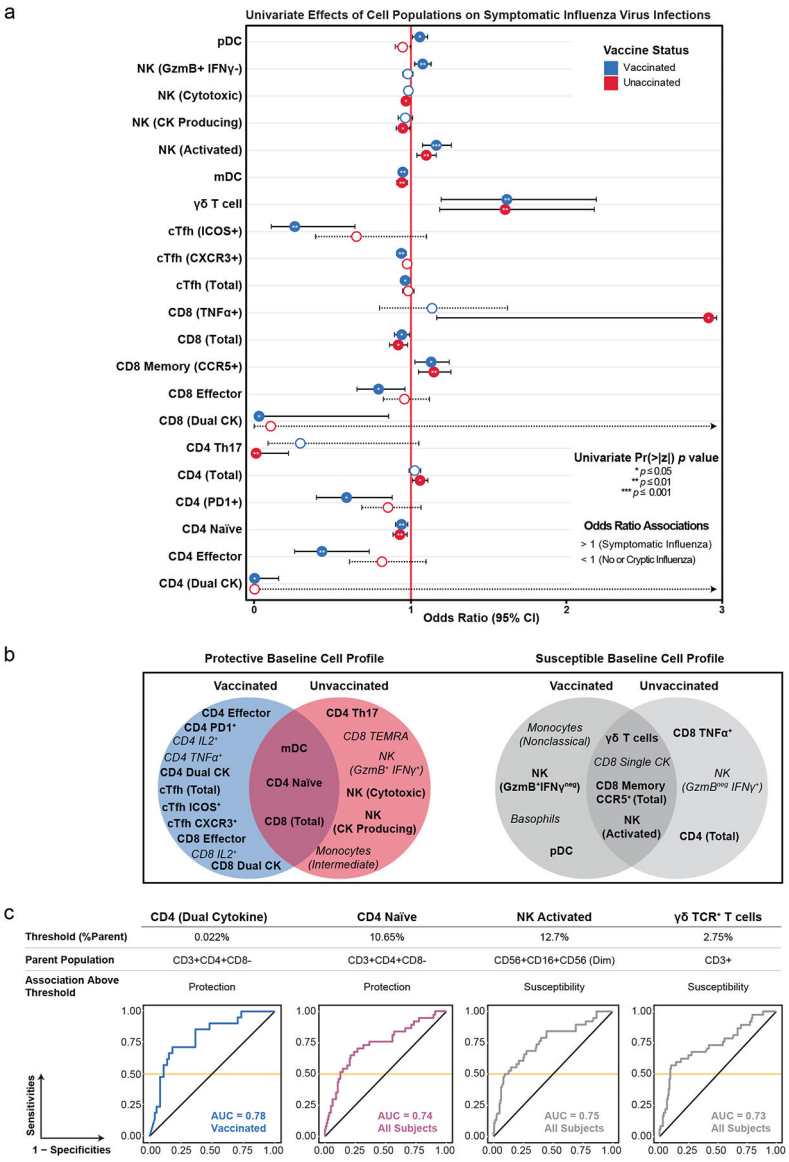

Figure 3: Univariate effects of cell populations on symptomatic influenza by vaccination status.

A) Univariate generalized logistic regression model (GLM) to determine individual effect of cell population frequency (% parent) effects on symptomatic influenza by vaccine status. Individual GLMs of unvaccinated participants generated from 98 DOF (uninfected/cryptic n=79, symptomatic n=19); GLMs of vaccinated participants generated from 108 DOF (uninfected/cryptic n=86, symptomatic n=22). GLM estimate values (logit) were transformed to Odds Ratio (OR; center circle) using the e-function and presented with associated 95% CI (bars). Cell populations with positive effects on symptomatic influenza have OR > 1 while cell populations with negative effects have OR < 1. Univariate significance determined from GLM Pr(>|z|) output (closed significant; open not significant) where z=estimate/SE. Significance defined as * $p \leq 0.05$; ** $p \leq 0.01$; *** $p \leq 0.001$. Exact Pr(>|z|) p values and FDR-adjusted q values reported in Supplementary Table 4. **b)** Baseline cell profiles associated with (left) protection from and (right) susceptibility to developing

symptomatic influenza by 2018 influenza virus vaccination status. Subjects with significant cell frequency outliers were determined by Grubbs' test ($p<0.05$) and removed from this analysis. All cell populations presented significant by one-sided Kruskal-Wallis (italicized) or both Kruskal-Wallis and univariate GLM (bold) evaluations. Exact p values reported in Supplementary Tables 3 and 4. **c)** Representative thresholds depicted as cell frequency (% parent) with associated ROC curves. A threshold defines the cell frequency at which the ROC curve sensitivity (true positives) equals 0.5 and represents the cutoff above which an individual factor correctly associates 50% of cases as protected or susceptible. AUC values indicate the overall quality (true vs false positives) of the individual measure in discerning protection or susceptibility.

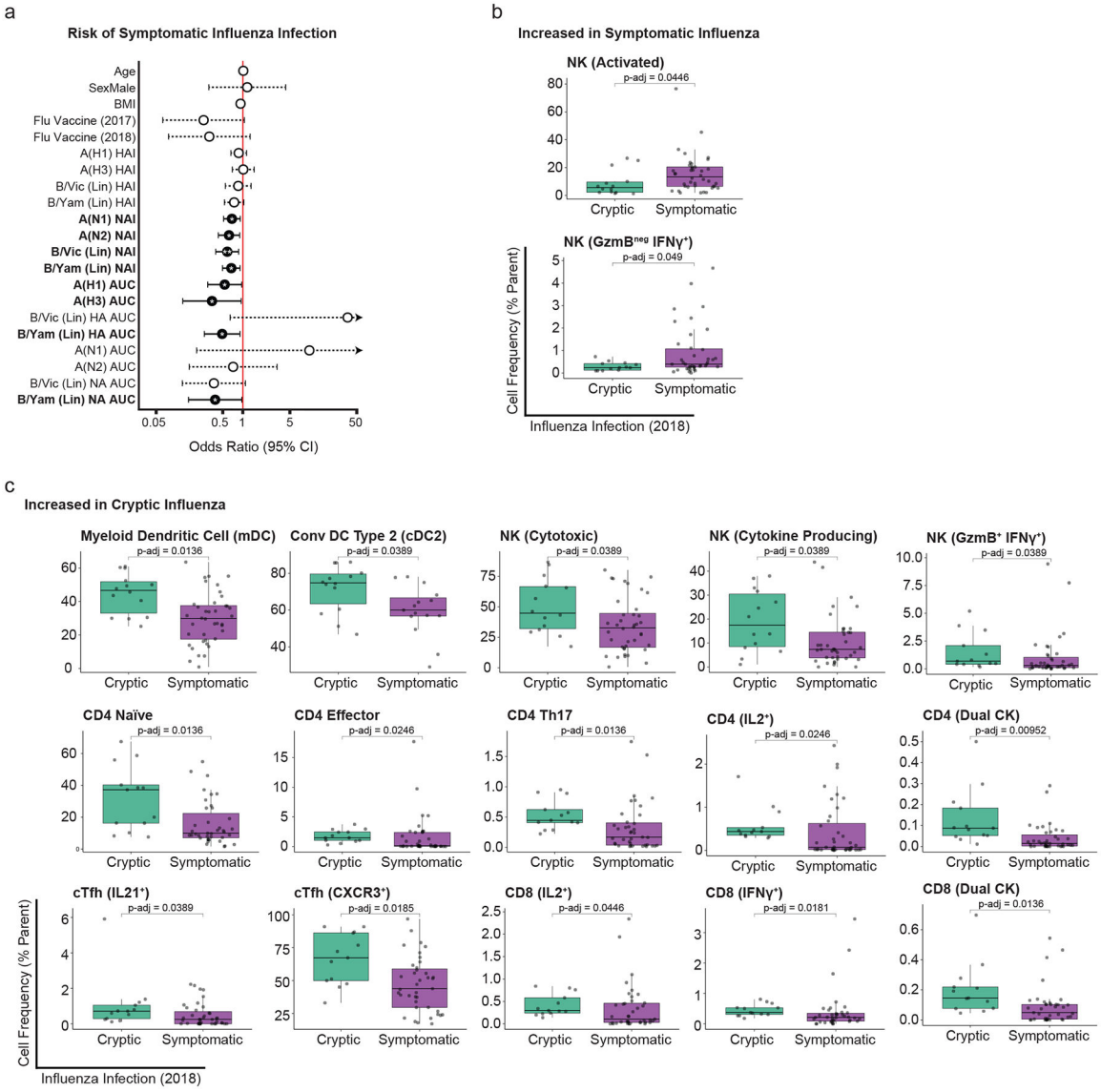

Figure 4: Cryptic infections are associated with unique cellular responses.

a) Relative risk of symptomatic infection among influenza virus-infected participants given demographic, serologic, or vaccine history covariates. GLM estimate values (logit) were transformed to Odds Ratio (OR; center circle) using the e-function and presented with associated 95% CI (bars). Univariate GLMs generated from 54 DOF (symptomatic n=41, cryptic n=14) except BMI (DOF = 46; symptomatic n=35, cryptic n=12). Significance determined from GLM Pr(>|z|) output where z=estimate/SE. Resulting two-tailed *p* values: Age *p*= 0.528, SexMale *p*= 0.827, BMI *p*= 0.24, Flu Vaccine 2017 *p*= 0.062, Flu Vaccine 2018 *p*= 0.111, A(H1) HAI *p*= 0.321, A(H3) HAI *p*= 0.945, B/Vic (lin) HAI *p*= 0.495, B/Yam (lin) HAI *p*= 0.091, A(N1) NAI *p*= 0.014, A(N2) NAI *p*= 0.015, B/Vic (lin) NAI *p*= 0.01, B/Yam (lin) *p*= 0.014, A(H1) AUC *p*= 0.041, A(H3) AUC *p*= 0.041, B/Vic (lin) AUC *p*= 0.082, B/Yam (lin) AUC *p*= 0.026, A(N1) NAI *p*= 0.249, A(N2) NAI *p*= 0.666, B/Vic NAI *p*= 0.076, B/Yam NAI *p*= 0.045. Not significant (blank); *$p \leq 0.05$.

b-c) Comparison of individual cell population frequencies (% parent) across cryptic and

symptomatic participants. Cell populations are grouped based on increased frequencies in **(b)** symptomatic or **(c)** cryptic influenza cases. In **(b)** NK Activated (cryptic n= 14 vs. symptomatic n= 40); NK GzmB^{neg}IFNγ^{+} (cryptic n= 13 vs. symptomatic n= 39) and **(c)** mDC, NK Cytotoxic, NK Cytokine Producing (cryptic n= 14 vs. symptomatic n= 40); cDC2 (cryptic n= 14 vs. symptomatic n= 15); NK GzmB^{+}IFNγ^{+}, CD4 Naïve, CD4 Effector, CD4 Th17, CD4 IL2^{+}, CD4 Dual CK, cTfh IL21^{+}, cTfh CXCR3^{+}, CD8 IL2^{+}, CD8 IFNγ^{+}, CD8 Dual CK (cryptic n= 13 vs. symptomatic n= 39). Lymphoid panel frequencies represent the average frequency (% parent) across virus (MOI = 4 A/Michigan/45/2015 H1N1pdm09 or A/Singapore/INFIMH-16-019/2016 H3N2) and peptide (1–5 μM /peptide pools containing M1, NP, PB1) stimulation groups. Boxes represent the median and 25th to 75th percentiles; whiskers indicate the minimum and maximum values no further than 1.5 times the interquartile (IQR). Means compared using two-sided Wilcoxon rank sum test with FDR adjustment with $q \leq 0.01$ achieving significance.

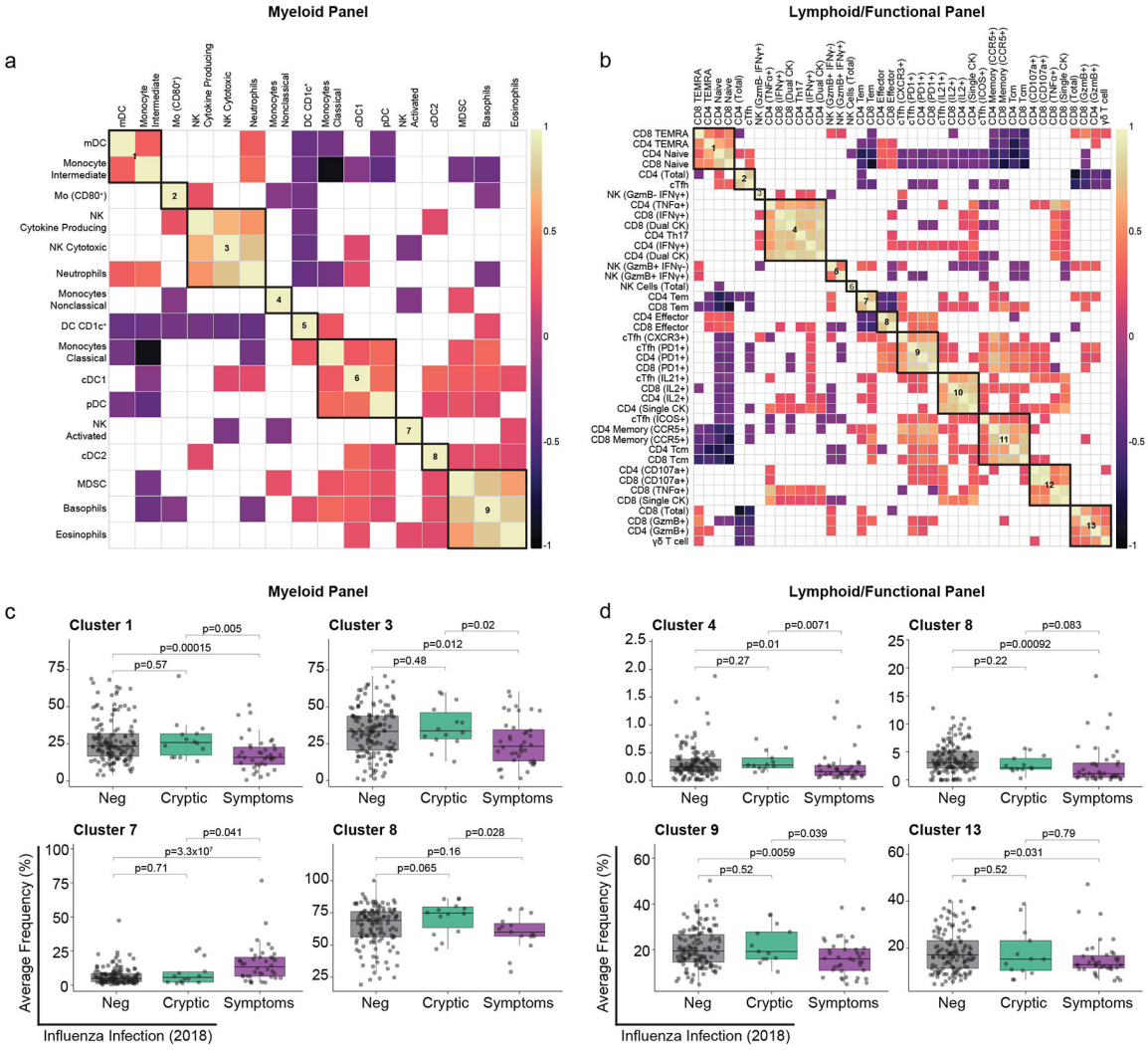

Figure 5: Co-regulated CMI and innate immune cell modules.

a-b) Co-regulated cell modules (“Clusters”) determined by average frequency (% parent) of individual cell populations from **(a)** myeloid or **(b)** lymphoid compartments with significant positive correlation (Pearson’s bivariate correlation). Lymphoid population frequencies calculated as average frequency across ICS stimulation conditions including peptide pools (M1, NP, PB1) and virus (A(H1N1), A(H3N2). *P* values were adjusted using false discovery rate (FDR; q) correction for multiple comparisons. Significance *q <0.1; **q<0.05; not significant (blank). **c-d)** Mean cell cluster frequencies from **(c)** myeloid or **(d)** lymphoid correlation matrices compared by influenza virus infection status (myeloid Cluster 1, 3, 7: uninfected (Neg) n=145 vs. cryptic n=14 vs. symptomatic n= 40; myeloid Cluster 8: Neg n=129 vs. cryptic n=14 vs. symptomatic n= 15; lymphoid Cluster 4, 8, 9, 13: Neg n=133 vs. cryptic n=13 vs. symptomatic n= 39) using two-sided Wilcoxon rank sum test. Boxes represent the median and 25th to 75th percentiles; whiskers indicate the minimum and maximum values no further than 1.5 times the interquartile (IQR).

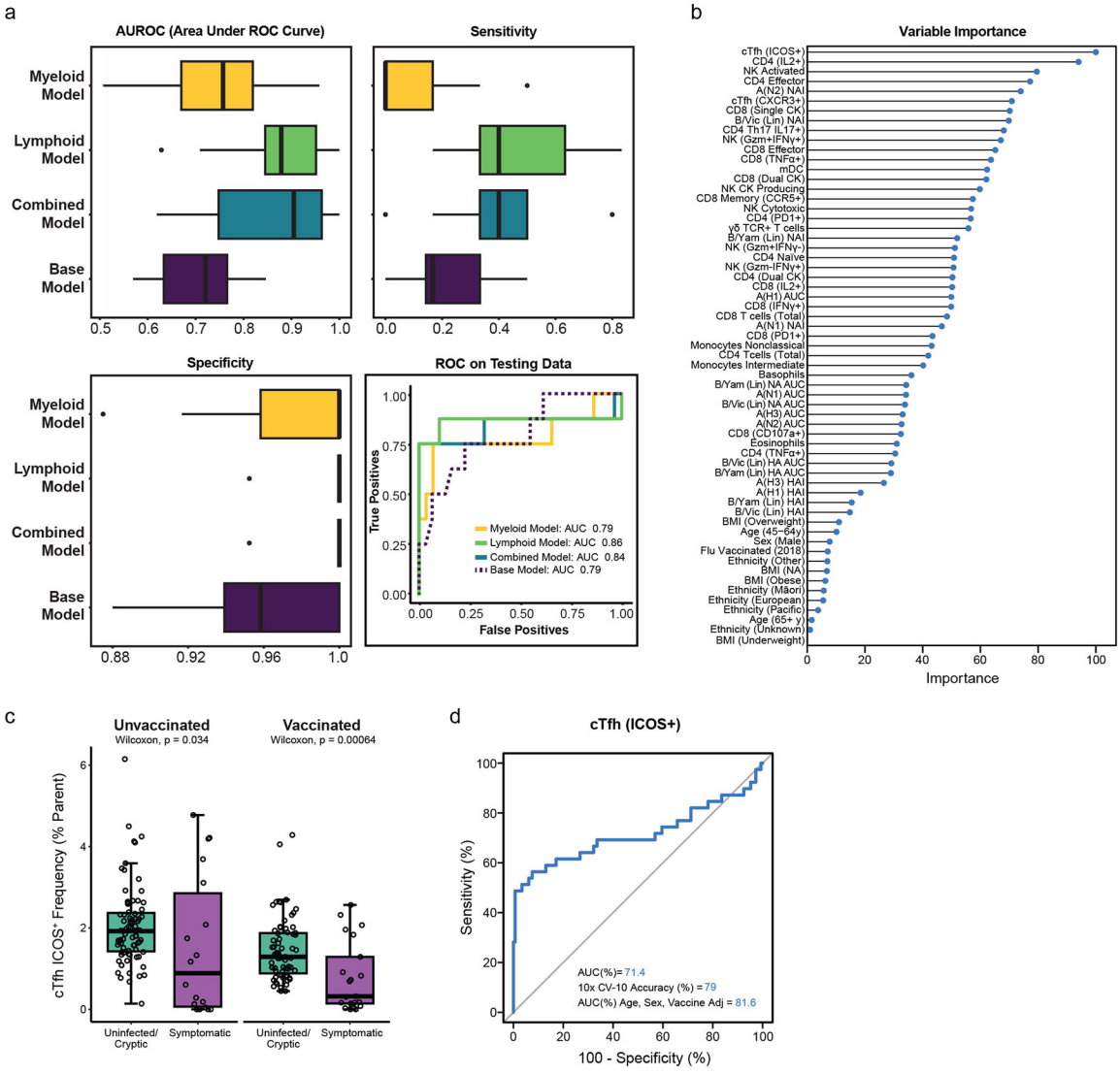

Figure 6: Decision tree model comparison.

a) Comparison of the Base (demographic factors + serology + vaccination status), Myeloid (base + myeloid panel cell populations), Lymphoid (base + lymphoid panel cell populations), and Combined (base + myeloid + lymphoid) random forest models built to categorize symptomatic and uninfected/cryptic influenza. Participants were split 80:20 into a training set (symptomatic cases n=31, uninfected/cryptic controls n=128) and testing set (symptomatic cases n=8, uninfected/cryptic controls n=33) ensuring equal proportions of cases and controls. Models were trained, tested, and cross-validated using 10-times cross-validation (10x CV-10). Sensitivity (true positive rate), Specificity (false positive rate) and AUROC (area under the receiver-operating characteristic curve) metrics and an out-of-sample evaluation of the models (bottom right) are provided. Boxes represent the median and 25th to 75th percentiles; whiskers indicate the minimum and maximum values no further than 1.5 times the interquartile (IQR). **b)** Relative importance of each baseline covariate in the Combined random forest Model; baseline covariates with high importance best categorize symptomatic and uninfected/cryptic influenza cases. Subjects

with significant cell frequency outliers were determined by Grubbs' test (p<0.05) and removed from this analysis. **c)** Mean cTfh (ICOS$^+$) cell frequency comparison between uninfected/cryptic and symptomatic influenza infection by 2018 influenza vaccine status using two-sided Wilcoxon rank sum test (unvaccinated symptomatic n=18 vs. unvaccinated uninfected/cryptic n=75; vaccinated symptomatic n=21 vs. uninfected/cryptic n=71). Boxes represent the median and 25th to 75th percentiles; whiskers indicate the minimum and maximum values no further than 1.5 times the interquartile (IQR). **d)** ROC curve generated from GLM predicting symptomatic influenza infection from cTfh (ICOS$^+$) cell frequency. AUC values from cTfh ICOS$^+$ GLM as univariate model, following 10x CV-10, and after age (years), sex, and 2018 influenza vaccine status adjustment.

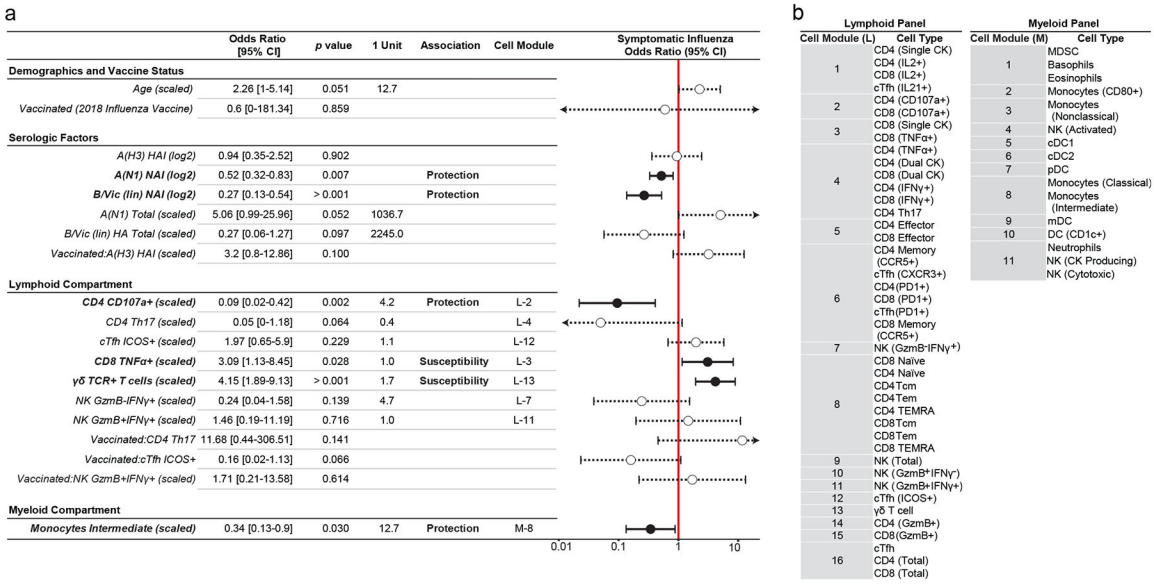

Figure 7: Baseline predictors of influenza virus infection susceptibility accounting for demographic, vaccination, serologic covariates, and cellular.

Multivariate generalized logistic regression model (GLM) predicting symptomatic influenza virus infection accounting for baseline demographics, vaccination status, serology, myeloid, and lymphoid covariates. **a)** Final logistic regression model with covariates by category predicting risk of symptomatic influenza (symptomatic n=39 and uninfected/cryptic n=161 participants). For covariate selection in the final model, baseline covariates with strong multicollinearity by variance inflation factor (VIF) assessment were excluded; single representative cell populations from each co-regulated cell cluster were included. Models comprising these covariates were compared by stepwise Akaike Information Criterion (AIC; forward and reverse) and Bayesian model averaging (BMA) to account for inherent model uncertainty arising from variable selection. Interaction terms denoted with a colon (:). Odds Ratio [95% CI] derived from exponential transformation of GLM estimate (logit) value; two-tailed *p* value significance determined from GLM Pr(>|z|) output (closed significant; open not significant) where z=estimate/SE. Variables were scaled as indicated based on their median and standard deviation values. The value for 1 Unit of change is indicated for each scaled value. Units for scaled values are years (Age), AUC (total antibody ELISA measures), log2 reciprocal endpoint titer (HAI; NAI), %parent frequency (cell populations). For example, for every increase of 12.7 years of age, there is an increase in the odds of susceptible influenza infection by 2.26, suggesting younger individuals are better protected. Association of significant baseline covariate predictors with symptomatic (Susceptibility) or uninfected/cryptic (Protection) influenza indicated. Subjects with significant cell frequency outliers were determined by Grubbs' test ($p<0.05$) and removed from this analysis. Cell Module column corresponds to **(b)** strongly correlated cell modules clustered based on absolute value of correlation. Significance *$p \leq 0.05$; **$p \leq 0.01$; ***$p \leq 0.001$.

Table 1:

Participant demographics

		Mean	Std Dev
Age (years)		43.8	12.6
BMI (kg/m^2)		27.5	5.6
Influenza Virus Infection Status (2018)		n	Percent
	Negative	151	73.3
	Positive	55	26.7
Influenza Virus Vaccination Status (2018)			
	Unvaccinated	98	47.6
	Vaccinated	108	52.4
Sex (assigned at birth)			
	Female	124	60.2
	Male	82	39.8
Ethnicity (participant-reported)			
	Asian	14	6.8
	European	171	83
	Māori	12	5.8
	Pacific	3	1.5
	Other	2	1
	Not Reported	4	1.9
BMI Group[†]			
	Underweight (<18.5)	1	0.5
	Normal Weight (18.5 - <25)	73	35.4
	Overweight (25- <30)	59	28.6
	Obese (≥30)	56	27.2
	Not Reported	17	8.3
Influenza Virus Strain			
	A(H1N1)	29	14.1
	A(H3N2)	5	2.4
	A(Untyped)	5	2.4
	B/Victoria lineage	1	0.5
	B/Yamagata lineage	1	0.5
	Cryptic	14	6.8
	Uninfected	151	73.3

[†]CDC-defined BMI groupings for adults ≥20 years (kg/m^2)